

ABSTRACT

Title of Thesis: DEVELOPMENT OF A FORCED
OSCILLATION TECHNIQUE FOR
DETERMINATION OF MAV STABILITY
CHARACTERISTICS

Daniel Peter Everson, Master of Science, 2005

Thesis directed by: Professor Darryll J. Pines
Department of Aerospace Engineering

This thesis presents the development and validation of a forced oscillation test technique for the determination of Micro Air Vehicle (MAV) stability characteristics. The test setup utilizes a scotch yoke mechanism to oscillate a MAV along a single axis at a fixed amplitude and frequency. The aerodynamic reaction forces to this sinusoidal perturbation are measured and converted into meaningful stability parameters. The purpose of this research is to demonstrate that forced oscillation testing is an effective means of measuring the stability parameters of a MAV. Initial tests show that the forced oscillation test process is returning results which match the expected trends. Comparison of the results to an analytical model of blade flapping shows that the experimental results are of the proper magnitude. It can be concluded from this research that forced oscillation testing is a feasible method for determining the stability parameters of MAVs.

DEVELOPMENT OF A FORCED OSCILLATION TECHNIQUE FOR
DETERMINATION OF MAV STABILITY CHARACTERISTICS

By

Daniel Peter Everson

Thesis submitted to the Faculty of the Graduate School of the
University of Maryland, College Park, in partial fulfillment
of the requirements for the degree of
Master of Science
2005

Advisory Committee:
Professor Darryll J. Pines, Chair/Advisor
Professor Norman M. Wereley
Professor Alison Flatau

© Copyright by
Daniel Peter Everson
2005

Acknowledgements

First I would like to thank my thesis committee: Dr. Darryll Pines, Dr. Norman Wereley, and Dr. Alison Flatau for taking the time to review and approve this thesis. I would especially like to thank Dr. Pines for serving as my advisor throughout my graduate studies. His patience with and confidence in my work has allowed my time at the University of Maryland to be a most enjoyable and rewarding experience. Special thanks are also due to Dr. Paul Samuel for his assistance in many aspects of this research. In the absence of Dr. Pines, Paul has been there to answer questions of widely varying importance on a daily basis.

Thanks also to all of the students in the rotorcraft center who at one time or another have offered their assistance in some way. In particular I would like to acknowledge Felipe, Jayant, Ben, and Tim, for showing me around the lab and teaching me many of the skills that I needed to complete this work. Also, thanks to Bernie and Howie for their guidance during many hours spent in the machine shop.

Lastly I would like to acknowledge my family and friends for their support during this process. Many of you have helped to either motivate me or distract me from my work in one way or another. Both have been very helpful from time to time. I am especially grateful to my parents for their love and encouragement, specifically my father for his persistence in pushing me towards my goal of completing this thesis.

Table of Contents

Acknowledgements.....	ii
Table of Contents.....	iii
List of Tables.....	v
List of Figures.....	vi
Chapter 1: Introduction.....	1
1.1 Background.....	1
1.2 Motivation.....	3
1.3 Objective.....	4
1.4 Organization of Thesis.....	6
Chapter 2: Literature Survey of System Identification Techniques for MAVs.....	8
2.1 Introduction.....	8
2.2 Estimation Charts.....	10
2.2 Finite Difference Approximations.....	11
2.3 Flight Testing.....	13
2.5 Forced Oscillation testing.....	15
2.6 Chapter Summary.....	17
Chapter 3: Forced Oscillation Testing, Theoretical Background.....	19
3.1 Introduction.....	19
3.2 Stability Derivative Approach.....	19
3.3 Bode Plot Representation Approach.....	26
3.4 Chapter Summary.....	28
Chapter 4: Forced Oscillation Testing: Experimental Setup.....	29
4.1 Introduction.....	29
4.2 Scotch Yoke Mechanism.....	31
4.3 Drive Motor Assembly.....	33
4.4 Force Balance.....	33
4.5 Signal Conditioner.....	35
4.6 Position Sensor.....	37
4.7 Data Acquisition System.....	38
4.8 Rotor Systems Under Consideration.....	38
4.8.1 Generic Co-axial.....	39
4.8.2 Teetering.....	40
4.8.3 Rigid Hub.....	41
4.9 Description of Blade Flapping Motion.....	42
4.10 Chapter Summary.....	45
Chapter 5: Forced Oscillation Testing: Test Procedure and Data Reduction.....	46
5.1 Introduction.....	46
5.2 Setup of Test Parameters.....	47
5.2.1 Forcing Frequency.....	47
5.2.2 Drive Motor Setting.....	48
5.2.3 Sampling Rate.....	50
5.2.4 File Organization.....	52

5.3	Tare Testing	53
5.4	Rotors-on Testing.....	54
5.5	Data Reduction.....	55
5.5.1	Use of MATLAB Program “mavplotDZ”	55
5.5.2	Use of MATLAB Program “mavavD”	58
5.6	Presentation of Results.....	63
5.6.1	Stability Derivative Representation	63
5.6.2	Bode Plot Representation.....	64
5.6.3	Presentation of Correlation Measurements.....	64
5.7	Chapter Summary	65
Chapter 6: Validation of Forced Oscillation Test Process.....		66
6.1	Introduction.....	66
6.2	Analysis of Test Results, Stability Derivative Perspective.....	67
6.2.1	Constraints on Evaluation of Stability Derivatives.....	67
6.2.2	Stability Derivative Measurement: Variation in Frequency	68
6.2.3	Stability Derivative Measurement: Variation in Amplitude.....	70
6.2.4	Stability Derivative Results: Co-Axial Rotor System	71
6.2.5	Qualitative Validation: Change in Rotor Collective.....	72
6.3	Analysis of Results, Bode Plot Perspective	75
6.3.1	Construction of Bode Plots	76
6.3.2	Teetering Rotor System	78
6.3.3	Rigid Hub Rotor System.....	84
6.4	Comparison of Data Representation Techniques.....	90
6.5	Analytical Validation of Test Results.....	91
6.5.1	Numerical Analysis of Blade Flapping Motion	91
6.5.2	Comparison of Numerical Analysis to Experimental Data.....	93
6.6	Application of Results.....	97
6.7	Additional Observations	98
6.8	Conclusions.....	101
Chapter 7: Concluding Remarks.....		103
7.1	Summary and Conclusions	103
7.2	Recommendations for Future Work.....	105
Appendix A: MATLAB Program Code, “mavplotDZ”		108
Appendix B: MATLAB Program Code, “mavavD”		113
Bibliography		117

List of Tables

Table 5.1	Oscillation Amplitude Setting	48
Table 5.2	Motor Setting to Achieve Desired Forcing Frequency	50
Table 5.3	Proper Sample Rate for Each Forcing Frequency	52
Table 6.1	Selection of Oscillation Amplitude.....	78
Table 6.2	Flapping Response from Analytical Calculations	95

List of Figures

Figure 3.1	Stability Derivative Assumed Response	21
Figure 4.1	Forced Oscillation Test Stand	30
Figure 4.2	Data Acquisition System	31
Figure 4.3	Scotch Yoke Mechanism	32
Figure 4.4	Force and Moment Balance	35
Figure 4.5	Investigation of Optimal Amplifier Gain Setting	37
Figure 4.6	Generic Co-axial Rotor System	40
Figure 4.7	Single Teetering Rotor	41
Figure 4.8	Blade Flapping Response to Perturbation in Forward Velocity	43
Figure 4.9	X-Force and Pitching Moment Response	44
Figure 5.1	Synchronous Averaging of Output Signal	56
Figure 5.2	Time Shift of Output Signal	57
Figure 5.3	Filtered Output Signal	58
Figure 5.4	Averaging of Multiple Tests	59
Figure 5.5	Subtraction of Tare Test from Rotors-on Test	60
Figure 5.6	First Term Fourier Series Approximation of Signal	61
Figure 5.7	Simultaneous Presentation of Multiple Tests	63
Figure 6.1	X_u vs. Forcing Frequency	69
Figure 6.2	X_u vs. Oscillation Amplitude	70
Figure 6.3	X_u vs. Collective Pitch Angle	73
Figure 6.4	Change in Rotor Collective: Qualitative Comparison	75
Figure 6.5	Change in Force Response for a Variation in Oscillation Amplitude	77
Figure 6.6	Bode Plot of Teetering Rotor X-Force Response	80
Figure 6.7	Correlation vs. Frequency for 11" Teetering Rotor	81
Figure 6.8	Response Signal for 11" Teetering Rotor at .6 Hz	82
Figure 6.9	Response Signal for 11" Teetering Rotor at 1.8 Hz	83
Figure 6.10	Bode Plot of Rigid Rotor Pitching Moment Response	86
Figure 6.11	Bode Plot of Rigid Rotor X-Force Response	87
Figure 6.12	Correlation vs. Forcing Frequency for 11" Rigid Rotor	88
Figure 6.13	Response Signal for 11" Rigid Rotor at .6 Hz	89
Figure 6.14	Flapping Angle vs. Time	94
Figure 6.15	Comparison of Analytical and Experimental Results	96
Figure 6.16	Inverted Rotor Comparison	100

Chapter 1: Introduction

1.1 Background

Recently there has been increasing interest in the development of hovering MAVs. The possible uses for hovering MAVs are limited only by the imagination, and many possible missions have already been proposed. These MAV specific missions pose a wide array of specific challenges. Often the prospective missions will include dynamic weather conditions, the presence of intricate obstacles and flight near or even potentially inside buildings. MAVs must be designed not only to handle these tasks but also do it autonomously. One of the most challenging aspects of MAV development is the design and implementation of autonomous or semi-autonomous flight control. A key requirement for the effective design and implementation of closed loop controllers and control strategies is an accurate model of the vehicle's dynamic response to control inputs and disturbances. Because of the unique nature of hovering MAVs, construction of an accurate dynamic model poses some unique challenges beyond those affecting full size rotorcraft.

Forced oscillation techniques have been widely used to determine aerodynamic stability derivatives for fixed wing vehicles in wind tunnel test facilities [1]. The predominant difference between those tests and the determination of stability derivatives for rotary wing vehicles is the time scale on which the new aerodynamic forces establish themselves following a perturbation in flight conditions. For fixed wing aircraft, the new forces on the aerodynamic surfaces and fuselage

establish themselves very quickly. For rotary wing aircraft there are similar changes in forces, but they occur on two different time scales. The new forces on the rotor and fuselage occur rather quickly, similar to a fixed wing aircraft. However, the reaction of the rotor to perturbations in flight conditions occurs more slowly. The concept behind stability derivatives assumes a constant coefficient system, which implies that the perturbation of forces occurs instantaneously. For rotary wing vehicles this is obviously not the case. However, this type of analysis can still be used if the perturbation occurs relatively slowly compared to the time it takes for the new aerodynamic forces to establish themselves. Because the MAVs to be used in this study operate at very high rotor RPMs, the reaction of the rotor is much quicker than that of a full-scale helicopter. However, great care must still be taken throughout the test process to ensure that the reaction of the rotor occurs very quickly with respect to the change in flight conditions caused by the forced oscillation.

Forced oscillation techniques can also be applied as a method of system identification, similar to the collection of flight test data. For the case of forced oscillation testing instead of inducing perturbations to the flight conditions of the vehicle using control inputs, as is done in traditional flight testing, the perturbations are caused by the forced oscillation motion. Analysis of forced oscillation testing in this manner uses Bode plots to represent the test results. A Bode plot consists of the gain and phase of the vehicle response plotted as a function of frequency. In this type of analysis it is not necessary to assume that the reaction of the rotor is instantaneous, because the phase delay of the response is considered. These Bode plots can then be approximated by transfer functions which describe the dynamic response of the

vehicle. Thus, there are two ways of analyzing the data recorded from a forced oscillation measurement, both of which will be considered herein.

1.2 Motivation

The primary motivation for the current research is to aid in the development of effective control systems for rotary wing MAVs. Because of the specific demands of projected missions for MAVs, the design of a capable controller promises to be a difficult task. In order to overcome the challenge of designing a controller for a mission capable MAV, the first step is to construct an adequate model of the flight dynamics of the proposed vehicle.

The current design process for rotary wing MAVs consists of designing a vehicle with the aerodynamics and lifting strategy as the primary focus. Once the vehicle is able to achieve flight, the designer is then faced with the issue of how to make it stable or at the very least flyable. The advent of a technique which is capable of studying the stability characteristics of a vehicle or rotor concept before the challenging “first flight” could be a powerful tool to the designer of a rotary wing MAV. In this case, the designer would have the ability to consider the stability parameters of the vehicle much earlier in the design process, thus reducing the risk of costly design changes forced by excessively unstable configurations.

There are two techniques which are traditionally used for determining a dynamic model for a modern rotorcraft. Neither of these techniques is currently capable of providing an accurate model for a rotary wing MAV. The first traditional method is to analytically calculate the model directly from the vehicle equations of motion using finite difference approximations. The second is to derive the model

from flight test data. Determining a vehicle's stability parameters directly from the equations of motion is a particularly difficult task in the case of an MAV. This is predominantly due to the absence of solid information regarding the dynamics of flight at low Reynolds numbers. Outfitting MAVs with the necessary sensory equipment to derive the stability derivatives from flight tests is also challenging due to their limited payload capacity. This problem is further complicated by the fact that MAVs are often difficult to fly in a consistent manner even with open loop remote control, and thus performing the maneuvers required to collect appropriate flight test data becomes a difficult task. For these reasons there is great interest in the ability to determine the stability derivatives of MAVs using experimental techniques in ground test facilities.

A technique which can experimentally achieve accurate system identification of a rotary wing MAV without the need for flight testing presents itself as an attractive tool in the process of MAV vehicle and control system design. For this reason there is sufficient interest in the use of forced oscillation testing as an alternative to analytical calculations or flight testing.

1.3 Objective

The primary focus of this research is the development and validation of a forced oscillation test procedure for the system identification of rotary wing MAVs. Specifically this thesis focuses on the creation of a capable test stand as well as the implementation of the necessary hardware required to obtain the required data. The data reduction process and analysis of the results are also addressed.

The current experimental setup consists of a test stand which is capable of producing a forced sinusoidal perturbation in the velocity of the vehicle along its X-body axis, about a hovering flight condition. This simple one degree of freedom perturbation was chosen in order to simplify the development and validation of the forced oscillation test procedure. The simple perturbation in forward velocity was chosen to initially validate the test process for two reasons. First, the response of the rotor to changes in forward velocity is one of the most important characteristics affecting the stability of a rotary wing vehicle in hover. This rotor response is discussed in more detail in section 4.9. Secondly, the mechanism needed to produce a perfect sinusoidal oscillation in velocity along the vehicle's X-axis is relatively simple to design and implement. If the forced oscillation test technique is proven to be effective for this simple case, it will justify the extension of the technique to other degrees of freedom.

The perturbation in velocity along the vehicle's X-axis is traditionally denoted u . The current design of the force balance can measure the aerodynamic X-force and pitching moment caused by this perturbation. From these measurements, M_u and X_u , the stability derivatives that describe the pitching moment response and X-force response, respectively, to a perturbation u , can be determined. Similarly, Bode plots which describe the frequency response of X-force and pitching moment to a perturbation in forward velocity can be constructed.

Three rotor systems have been considered for initial testing and validation. The first is a generic co-axial MAV without a lateral control system, based on the design of the University of Maryland's co-axial rotary wing MAV, MICOR [2], [3],

[4]. The second is a simple 11 inch diameter teetering rotor. The final rotor system is an 11 inch diameter rotor with similar properties to the teetering rotor, only the rotor hub is rigid in nature. The objective of this research is to use the three rotor systems described above to investigate the forced oscillation test procedure and validate the method as an accurate way to identify the stability parameters of a rotary wing MAV.

1.4 Organization of Thesis

Each of the following chapters is summarized below.

1. **Chapter 2: Literature Survey of System Identification Techniques for MAVs.** This chapter will give a summary of the previous research done in the area of system identification with potential applications to MAVs. Special attention is paid to the use of forced oscillation testing for the determination of stability parameters of fixed wing aircraft. This previous work on forced oscillation testing serves as the starting point for the forced oscillation testing of MAVs.
2. **Chapter 3: Forced Oscillation Testing, Theoretical Background.** This chapter will discuss the theory necessary to implement a forced oscillation test procedure. Forced oscillation testing will be considered from two perspectives, stability derivative analysis and Bode plot analysis. The governing equations for reducing test data to meaningful values for each of these two perspectives will be developed and presented.
3. **Chapter 4: Forced Oscillation Testing: Experimental Setup.** This chapter will describe the current test setup, which has been developed for the forced oscillation testing of MAVs. Each of the components utilized in the test step

is described and their individual contributions to the overall test process are discussed. The example test rotors which have been fabricated for initial testing are also presented and the characteristics of each are discussed.

4. **Chapter 5: Forced Oscillation Testing: Test Procedure and Data Reduction.** This chapter will present the procedure which is currently in use for the forced oscillation testing of MAVs. The proper selection of each test parameter is described, and the necessary steps for data collection are listed. This chapter also discusses the reduction of test data into meaningful stability parameters using MATLAB.
5. **Chapter 6: Validation of Forced Oscillation Test Process.** This chapter will discuss the initial tests which have been performed using the previously described test setup and procedure. The goal of this chapter is to provide a validation of the test process. Results from the testing of several example rotor systems are presented and the implications of the results are considered. Analysis of the initial test results is presented as a qualitative validation of the test process. This chapter also details an analytical model of the flapping response of one of the example rotor systems. This analytical model is then used to provide a quantitative validation to support the experimental results.
6. **Chapter 7: Concluding Remarks.** This chapter presents a summary of the work done and results produced from this research. Suggestions for future work in this area are also presented.

Chapter 2: Literature Survey of System Identification

Techniques for MAVs

2.1 Introduction

There has been a lot of previous work concerning the system identification of aerospace vehicles, both fixed and rotary wing. A variety of identification methods have been developed and validated, each with their own useful application. In the case of MAVs however, many of these methods prove to be only marginally useful. The goal of system identification is to properly identify the response characteristics of the vehicle to either a control input or a change in flight condition. The evolution of system identification and its applications to flight vehicles is described by Hamel and Jategaonkar [5]. System identification results can be applied in all phases of vehicle design, from initial estimates based on vehicle parameters, to final results found from flight tests of the finished product. Another aspect is the ability to identify the contribution of individual vehicle components to the total system response. For the case of a full scale rotorcraft there are four basic approaches to approximating the system parameters of the vehicle. These approaches include:

- The use of equations or charts to approximate vehicle stability
- The use of finite difference approximations to model vehicle response
- Flight testing of vehicle to obtain stability characteristics

- Forced oscillation testing on the ground

A synopsis of these techniques is given below and a survey of the relevant literature is presented in detail in the following sections.

The most basic approach to approximating a vehicle's response characteristics is to use equations or charts which approximate the contributions of each vehicle component to the total vehicle stability response. Using this method the stability characteristics of a vehicle can be predicted from concept through construction simply by knowing the values of the vehicle parameters. This process can provide a simple estimate without the need for advanced analysis or the assistance of a digital computer.

A more computationally complex method of determining the stability parameters of a rotorcraft is to use finite difference approximations to calculate the necessary characteristics directly from the vehicle equations of motion. While this method requires more time and computing power, it has several advantages over the use of charts or approximation equations. By developing sophisticated equations of motion to describe the vehicle and additional degrees of freedom, this method can account for more complicated vehicle configurations and designs than the previous approximation technique.

If a completed flight worthy vehicle is available the system parameters can be identified directly from flight testing. If adequate control inputs are applied and the vehicle response is measured the vehicle response characteristics can be identified. While this is a very useful technique, it is limited by the need for a completed flight test vehicle as well as the ability to collect sufficient flight test data.

A final method which in the past has been applied primarily to fixed wing aircraft is forced oscillation testing. In this method a vehicle model is placed inside a wind tunnel and forced to oscillate. The aerodynamic force response to this oscillation is measured and can then be reduced to give the stability characteristics of the vehicle. While this method has its limitations as well, due to the small size of a MAV and the difficulty in utilizing the other techniques above, it is particularly applicable in the case of small scale rotorcraft testing.

2.2 Estimation Charts

The development of estimation charts stems from the use of historical information as well as analysis of simple helicopter theory to predict the stability characteristics of a helicopter based on the design values of its components. For a traditional helicopter the primary contribution to the stability characteristics come from the main and tail rotors. By differentiating the equations for the aerodynamic coefficients and flapping angles, charts can be prepared which predict the contribution of the rotors to the vehicle response. Charts of this type have been developed by Amer and Gustafson [6]. A similar but slightly more modern adaptation of use of charts technique is described by Prouty [7]. In this case, rotor performance charts are used to predict the changes in rotor forces due to changes in flight conditions.

The primary advantage of the methods described above is that they enable a designer to predict the stability characteristics of a vehicle long before any of the vehicle components have been constructed. This method is also very simple to use when sufficient computing power is not available. This type of estimation was used extensively before the advent of the modern computer. Because of the increase in

digital computing technology, estimation charts are now an outdated means of vehicle parameter estimation. These methods can still prove useful however for quick calculations or to check the output of more sophisticated estimations.

Estimation charts and equations are also of very little use in the system identification of MAVs. Even though the previously cited methods were designed to be applicable over a large range of helicopter sizes they are of little use at the MAV scale. Because of the extreme discrepancy in size between an MAV and a full size rotorcraft, the physics which govern flight at the two different scales are quite different. For this reason estimation charts and equations serve as little more than a qualitative look at or gross approximation of the expected rotor response of a rotary wing MAV.

2.2 Finite Difference Approximations

The current method primarily used to analytically identify vehicle system parameters is to calculate them directly from the equations of motion using finite difference approximations. This is a very powerful numerical technique which has proven even more useful in recent years due to the advent of powerful digital computers. A more detailed discussion of the theory behind finite difference approximations is given by Smith [8]. An additional survey of the development and application of finite-difference techniques is provided by Schlager and Schneider [9]. The application of finite difference approximation to the development of aerodynamic databases is presented by Jateganokar and Thielecke [10]. An advantage of this technique is that equations of motion which include many degrees of freedom can be used. This is an especially attractive capability when studying rotorcraft, which generally have many

coupled degrees of freedom. Also, because the technique is not limited to a simple conventional single main rotor helicopter advanced configurations can be studied.

A general application of the use of finite difference approximations to the simulation of helicopter dynamics is provided by Webster et al. [11]. Because of the ability to consider many degrees of freedom and coupled equations, finite difference approximations have also been used to study more complicated aerodynamic phenomena. Ballhaus and Goorjian have used the technique to study unsteady flow regimes [12]. The ability to analyze complicated models is especially useful in studying rotary wing dynamics. A rotor design methodology which includes structural degrees of freedom is presented by Celi [13]. Another example is a study of helicopter flight dynamics including a wake model, performed by Theodore and Celi [14].

Although the use of finite difference approximations has proven to be an effective method for determining the stability characteristics of full size rotorcraft, they once again are not particularly useful at the MAV scale. In order for the approximations to be accurate, an appropriate model of the aerodynamic forces acting on the vehicle must be constructed. While the aerodynamics of a full size helicopter are well documented, this is not the case for rotary wing MAVs. Once again, the physics governing flight at the MAV scale are quite different than those governing the flight of a full size rotorcraft. Because an appropriate low Reynolds number aerodynamic model is not available, using the finite difference approximation method to determine the stability parameters of an MAV will only provide, at best, a general insight into the system identification of MAVs.

2.3 Flight Testing

Of the currently available methods for system identification, flight testing has shown to be the most prominent for modern rotorcraft. If a flight worthy prototype is available, properly conducted flight tests can accurately determine the system parameters of a vehicle over a large frequency range. The ability of flight testing to provide the necessary data for high bandwidth control design is presented by Tischler [15]. The fundamental idea behind flight test based system identification is to use control inputs to perturb the vehicle about a steady state flight condition and measure the vehicle response. From the response of the vehicle to a known input, the stability parameters of the vehicle can be determined. There is extensive literature detailing flight test procedures as well as the collection and analysis of the resulting data. The evolution of system identification flight testing to its current capability is discussed by Hamel and Jateganokar [5], [16]. The role of flight testing as applied to the parameter identification of rotorcraft is further discussed by Chen and Tischler [17]. Tischler has also conducted additional research on available methods for system identification flight testing [18]. An instructional description of the application of system identification flight testing to rotary wing vehicles is provided by Tischler et al. [19].

Much of the current research in system identification flight testing utilizes frequency domain analysis to extract the stability parameters of rotorcraft from flight test data. An application of frequency domain modeling for the control of unmanned air vehicles (UAVs) is given by Theodore et al. [20]. Other researches have also

shown the ability to perform system identification in the time domain. Time domain analysis for the control design of rotary wing UAVs is discussed by Shim et al. [21].

Recent work has been conducted by Mettler et al. to determine the stability characteristics of small scale rotary wing vehicles [22], [23]. While this research does not yet display the capability to perform system identification flight testing for MAVs, the successful application to less than full scale rotorcraft is a promising result. This research utilizes CIFER, a software package developed to extract vehicle stability parameters from flight test data. CIFER was originally developed to assist in the system identification of full size helicopters but has proven to be a valuable tool in the identification of small scale rotary wing vehicles as well as UAVs. The software package utilizes frequency domain, nonparametric analysis which has shown to be especially well suited in dealing with the rapid response and nonlinear characteristics of small scale rotorcraft. Additional research on the system identification of small unmanned helicopters has also been performed by Kim et al. [24]. Lee et al. have conducted research on small scale rotorcraft involving automated flight testing [25].

System identification from flight test data has proven to be a useful tool to the helicopter designer, but there are a few drawbacks which hinder its use in the case of rotary wing MAVs. The primary drawback is that to be properly implemented the method requires numerous channels of flight data. This requirement is detailed by Tischler et al. [19]. As additionally discussed by Mettler, this data must be of sufficient quality so that the results are not obscured by measurement noise [22]. While this is not necessarily an issue for larger rotorcraft, it is most certainly a

concern in the case of MAVs. The necessary instrumentation to deliver sufficient in-flight measurements is readily available for full size aircraft, but fitting this hardware to a MAV is a challenge. The payload of current MAVs is very limited [2]. For this reason the standard sensors must be reduced in size and weight while still delivering data of sufficient quality.

The other issue which makes flight testing difficult to apply to MAVs is the need for complete flight worthy vehicles as a test platform. Because of the rapid frequency response and generally unstable dynamics of bare airframe MAVs, it can be difficult to develop vehicles worthy of flight testing. Also, flight testing does not allow for the testing of individual components such as rotor systems if they are not part of a completed flight vehicle.

2.5 Forced Oscillation testing

The use of forced oscillation testing has been well documented in literature for the system identification of fixed wing aircraft in wind tunnels. A paper detailing a variety of different forced oscillation techniques and their applications is provided by Schuler et al. [1]. These techniques consist of using a mechanical mechanism to induce an oscillatory motion to a scaled vehicle model. By placing the model in a wind tunnel and measuring the aerodynamic reaction forces caused by the induced oscillation, the stability parameters of the vehicle can be determined. A summary of several more forced oscillation testing procedures is provided by von der Decken et al. [26]. An additional forced oscillation mechanism for the forced oscillation testing of stability derivatives in roll is given by Burt [27]. Orlick-Ruckemann et al. additionally address the technique for the application to unconventional

configurations [28]. One of the advantages of these procedures is that they are experimental methods similar to flight testing, but are preformed in a ground test facility. For this reason a fully flight worthy vehicle is not required for testing. Models of early prototypes can be tested before a vehicle which is capable of piloted flight has been completed.

More recent research has also been conducted using forced oscillation testing. Alemdarogul et al. provide a more modern outlook on the capabilities of forced oscillation testing [29]. There has been significant research on the development of improved capabilities and mechanisms over those described in the historical references. Hanff et al. describe the development of a large amplitude, high rate oscillation system [30]. A six degree of freedom simulation based on forced oscillation testing is discussed by Kalviste [31]. Progress has also been made for forced oscillation testing in the transonic regime as described by Piatak and Cleckner [32]. Additional research has been conducted involving the use of forced oscillation testing to measure unsteady aerodynamics. Work in this area has been detailed by Kay [33] as well as by Murphy and Klein [34]. Lastly there have been several studies in recent years examining the validity of different aspects of forced oscillation testing. Uselton and Uselton have studied the validity of small amplitude forced oscillation techniques [35]. The validity of forced oscillation testing for the measurement of unsteady aerodynamic parameters has been researched by Murphy and Klein [36].

The primary shortcoming of forced oscillation testing is that the parameters which can be identified from each test are limited by the mechanism used to oscillate the vehicle model. This limitation is discussed in more detail by Orlick-Ruckemann

[37]. Often a separate apparatus is required to perturb the vehicle about each degree of freedom. Also, the hardware used to measure the aerodynamic response forces can limit the possible results if the apparatus can not measure reaction forces and moments about each vehicle degree of freedom.

Forced oscillation testing does however present itself as a useful tool for rotary wing MAV system identification. Because of the small size of MAVs, scaled models are not required. Rather, a full size version of the vehicle can be tested. The other favorable characteristic of forced oscillation testing is that a flight worthy vehicle is not needed for testing. Because of the rapid response and frequently unstable dynamics of rotary wing MAVs they can be difficult to fly without significant piloting skill or an implemented flight control system. Since free flight is not required for forced oscillation testing, early prototype vehicles or rotor systems can be tested. The results from these tests can then be used to suggest modifications to the vehicle or to design an appropriate flight control system to make the vehicle more stable prior to flight testing.

2.6 Chapter Summary

In summary, much research has been performed previously in the field of system identification of rotary wing vehicles. Unfortunately, many of the techniques which have previously been developed are not currently applicable for use on MAVs. Forced oscillation testing of fixed wing aircraft in wind tunnels has also been well documented. It is possible that an extension of forced oscillation wind tunnel testing may prove to be a useful tool for the system identification of rotary wing MAVs.

The following chapter will present the theoretical background for forced oscillation testing. This background will be presented from two different perspectives, and the applications to the testing of MAVs will be discussed.

Chapter 3: Forced Oscillation Testing, Theoretical Background

3.1 Introduction

Forced oscillation testing is essentially a simplified version of the standard system identification techniques used in flight testing. For a given forced oscillation test a sinusoidal perturbation in one of the vehicles flight conditions is induced. The aerodynamic reaction to this perturbation is then measured. The relation of the output measurement to the input perturbation is then determined. This is analogous to the techniques used in standard system identification, only the test case is greatly simplified. Because only one flight condition is perturbed and both the input and the output are assumed to be purely sinusoidal, the analysis of the resulting data is far less complicated.

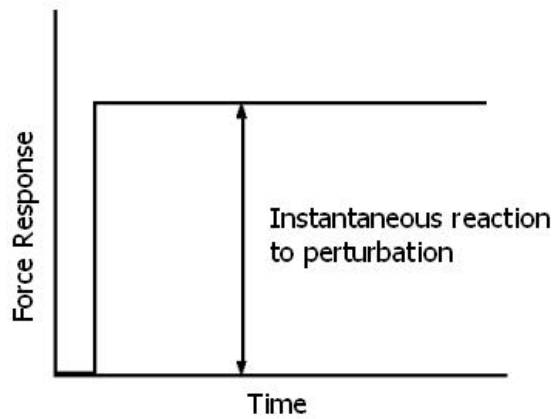
For the current research a simple one degree of freedom perturbation in velocity along the X-axis of the vehicle was chosen. The reasons for this choice are discussed in detail in section 1.3. Because only a single degree of freedom is considered in this research the analysis of the vehicle response is greatly simplified. In the following theoretical development please note that only motion along the X-axis is considered.

3.2 Stability Derivative Approach

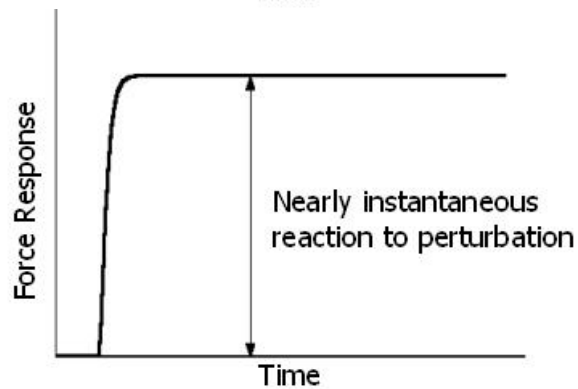
As discussed previously, the use of stability derivative approximations has some limitations for the applications to rotary wing vehicles. Namely the response of the

rotor system to perturbations is generally slower than the response of traditional aerodynamic surfaces. For this reason, stability derivatives are generally a better approximation of the response of traditional aircraft than they are for rotorcraft. Because the theoretical development of stability derivatives assumes an instantaneous reaction, care must be taken to insure that perturbations in flight conditions can be considered slow with respect to the reaction of the rotor. Figure 3.1 depicts the assumption made by stability derivative approximations as well as representative responses of a fixed wing aircraft and a rotorcraft.

**Assumption Made by
Stability Derivative
Approximation**



**Representative
Response of
Traditional Aircraft**



**Representative
Response of Rotary
Wing Aircraft**

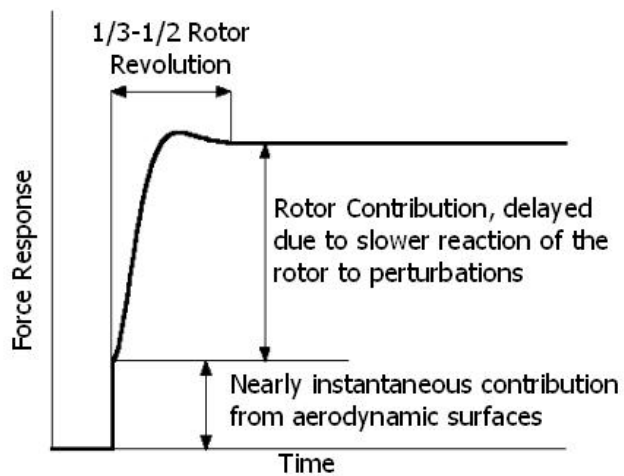


Figure 3.1 Stability Derivative Assumed Response

The theory utilized for the development of a stability derivative approximation assumes that the vehicle in question is initially in a trimmed flight condition. The stability derivative equations then predict the change in forces that are induced by

changes to the trimmed condition. The aerodynamic forces and moments acting on a vehicle while that vehicle is in trimmed flight can be expressed as a function of the flight parameters for that trim condition. Because the vehicle is in trimmed flight these flight parameters are considered constant. For small perturbations in flight conditions about these constant values the new force acting on the vehicle along the X-body axis can be expressed as a combination of the force on the vehicle at trim, X_T , and the change in that force due to the perturbation, ΔX

$$X = X_T(u, v, w, p, q, r, \theta_0, \dots) + \Delta X \quad (3.1)$$

where u , v , and w are the trim values for vehicle velocity along each body axis and p , q , and r are the trim values of rotational rates about each of the axes. Using a Taylor series expansion ΔX can be represented as the summation of the partial derivatives of X with respect to each flight condition, where these derivatives are calculated about the trim condition. Thus, ΔX can be expressed as

$$\Delta X = \frac{\delta X}{\delta u} \Delta u + \frac{\delta X}{\delta v} \Delta v + \frac{\delta X}{\delta w} \Delta w + \dots \quad (3.2)$$

where Δu , Δv , etc. are small perturbations to the trimmed flight conditions u , v , etc. The partial derivatives in the equation above are traditionally referred to as stability derivatives. Using a more concise notation, these stability derivatives are expressed as a force or moment component with a subscript indicating the variable with respect to which the component is being differentiated. For example, $\frac{\delta X}{\delta u}$ becomes the stability derivative X_u . Using this new notation, the simplified expression for ΔX is

$$\Delta X = X_u \Delta u + X_v \Delta v + X_w \Delta w + X_p \Delta p + \dots \quad (3.3)$$

In order to determine the stability derivatives of a vehicle experimentally, a forced sinusoidal oscillation can be used to impart a prescribed small perturbation to a steady flight condition. By measuring the resulting change in aerodynamic force, the appropriate stability derivative can be determined. For a prescribed sinusoidal oscillation in the X direction, position of the vehicle is given by

$$x(t) = A_0 \sin(\omega t) \quad (3.4)$$

where A_0 is the amplitude of the forced oscillation and ω is the prescribed angular frequency. Differentiating and twice differentiating this equation yields the velocity and acceleration of the vehicle. These equations give us the perturbation values for velocity and acceleration of the vehicle along the X axis. The perturbations are given as,

$$\begin{aligned} \dot{x}(t) &= A_0 \omega \cos(\omega t) = \Delta u \\ \ddot{x}(t) &= -A_0 \omega^2 \sin(\omega t) = \Delta \dot{u} \end{aligned} \quad (3.5)$$

The total force along the X axis, as measured by the force balance during a rotors-on test, can be represented as the sum of the aerodynamic force produced by the vehicle and the force produced by the inertia of the vehicle and the force balance itself.

$$F_T = F_I + F_A \quad (3.6)$$

The purely aerodynamic forces can be separated from the total measured force response by subtracting the inertia forces from the total force measured by the force balance.

$$F_A = F_T - F_I \quad (3.7)$$

Experimentally this is done by first running a tare test with the rotors off to determine the forces caused solely but the inertia of the vehicle F_I and then running the test again with the rotors on to determine the total force response F_T .

Conventionally, the aerodynamic force acting on the vehicle can be represented by the sum of a constant term, a term proportional to the vehicle velocity, and a term proportional to the vehicle acceleration.

$$F_A = A + Bu + C\dot{u} \quad (3.8)$$

The constant term A is dropped from the equation as the vehicle is operating about a trimmed hover condition and it is therefore assumed that before perturbations are introduced there are no forces acting on the vehicle. For the test case u and \dot{u} are small perturbations about a trimmed hover condition, thus they are more accurately represented as Δu and $\Delta \dot{u}$.

$$F_A = A + B\Delta u + C\Delta \dot{u} \quad (3.9)$$

If only the component of F_A that acts along the X -body axis, F_{A_x} , is considered it becomes apparent that B is actually the stability derivative for force in the X direction due to a perturbation in u , X_u . Similarly, $C = X_{\dot{u}}$. While the derivative $X_{\dot{u}}$ is not of particular interest from a dynamics point of view, it is retained throughout this analysis for thoroughness. The new notation for aerodynamic force along the X -body axis is now

$$F_{A_x} = X_u \Delta u + X_{\dot{u}} \Delta \dot{u} \quad (3.10)$$

Inserting the expressions for u and \dot{u} from equation 3.5, as prescribed by the forced oscillation gives an equation for the aerodynamic force in the X direction due to a perturbation in X velocity.

$$F_{A_x} = X_u A_0 \omega \cos(\omega t) - X_{\dot{u}} A_0 \omega^2 \sin(\omega t) \quad (3.11)$$

Returning to equation 3.9, the aerodynamic force as measured by the force balance, the measured force response can be represented by a Fourier series approximation.

$$F_{A_x} = F_S + F_C + HHT \quad (3.12)$$

where F_S and F_C are the first sine and cosine terms of the Fourier series expansion of the signal and HHT represents the higher harmonic terms. The higher harmonic terms are dropped from the equation due to the assumption that the aerodynamic force response of the vehicle will stem directly from the perturbation to flight conditions imparted by the forced oscillation. Utilizing the dependence of F_S and F_C on the known forced oscillation frequency

$$F_S = |F_S| \sin(\omega t) \quad (3.13)$$

$$F_C = |F_C| \cos(\omega t) \quad (3.14)$$

where $|F_S|$ and $|F_C|$ are the magnitudes of the in-phase and quadrature components of the first harmonic term of the Fourier series expansion respectively. Setting equations 3.11 and 3.12 equal to each other and inserting equations 3.13 and 3.14 yields,

$$F_{X_A} = |F_S| \sin(\omega t) + |F_C| \cos(\omega t) = X_u A_0 \omega \cos(\omega t) - X_{\dot{u}} A_0 \omega^2 \sin(\omega t) \quad (3.15)$$

Equating the sine and cosine terms from each side of the equation and solving for the stability derivatives yields

$$\begin{aligned}
X_u &= \frac{|F_c|}{A_0 \omega} \\
X_{\dot{u}} &= \frac{|F_s|}{A_0 \omega^2}
\end{aligned}
\tag{3.16}$$

Thus, by measuring the in-phase and quadrature aerodynamic force response of the vehicle while specifying the parameters of the prescribed forced oscillation the stability derivatives X_u and $X_{\dot{u}}$ can be obtained.

Because the force balance is set up to measure both the force in the X direction and the pitching moment of the vehicle M , similar relations hold for the derivatives of pitching moment for perturbations in u , given as

$$\begin{aligned}
M_u &= \frac{|M_c|}{A_0 \omega} \\
M_{\dot{u}} &= \frac{|M_s|}{A_0 \omega^2}
\end{aligned}
\tag{3.17}$$

3.3 Bode Plot Representation Approach

As stated in section 1.1, the aerodynamic force response data can also be represented in the form of gain and phase as a function of frequency. This type of representation is more commonly known as a Bode plot. Forced oscillation testing can also be used to construct a Bode plot of the vehicle response. Essentially, each forced oscillation test is capable of providing one point on both the gain and phase portions of a Bode plot. Thus, by performing forced oscillation tests over a range of frequencies a Bode plot of the vehicle response can be constructed point by point. The development of the theory used to construct a Bode plot from the data follows a similar derivation to that used in the stability derivative representation.

Simple dynamics theory gives that for a sinusoidal input to a mechanical system, the steady state system response will occur at the same frequency, but may contain a certain amount of phase delay. The input to the system is given by the velocity perturbation to the trimmed hover condition.

$$\dot{x}(t) = A_0 \omega \cos(\omega t) \quad (3.18)$$

The output of the system is the aerodynamic force in the X -direction, F_{A_x} .

$$F_{A_x} = a \cos(\omega t - \psi) \quad (3.19)$$

where a is the amplitude of the output, and ψ is the phase delay between the input and the output. Returning to the Fourier series representation of the aerodynamic force reaction, we have already established

$$F_{A_x} = F_S + F_C + HHT \quad (3.20)$$

where

$$F_S = |F_S| \sin(\omega t) \quad (3.21)$$

and

$$F_C = |F_C| \cos(\omega t) \quad (3.22)$$

Converting from the in Fourier series representation to the equivalent magnitude and phase representation, the gain and phase of the output are given by

$$a = \sqrt{|F_S|^2 + |F_C|^2} \quad (3.23)$$

$$\psi = \tan^{-1} \left(\frac{|F_S|}{|F_C|} \right) \quad (3.24)$$

In order to construct a Bode plot of the results it is necessary to calculate the gain of the system. The gain is simply the ratio of the output amplitude to the input amplitude, or

$$\frac{\text{output amplitude}}{\text{input amplitude}} = \frac{a}{A_0\omega} \quad (3.25)$$

Inserting the expression for output amplitude from equation 3.23 the gain and phase points corresponding to the frequency of forced oscillation on the Bode plot of the system for a given forcing frequency can be expressed as,

$$\text{gain} = \frac{\sqrt{|F_s|^2 + |F_c|^2}}{A_0\omega} \quad (3.26)$$

$$\text{phase} = \tan^{-1}\left(\frac{|F_s|}{|F_c|}\right) \quad (3.27)$$

3.4 Chapter Summary

In this chapter the theoretical development of forced oscillation testing has been presented. The equations necessary to convert the dynamic measurements from forced oscillation testing to stability derivatives have been given. The extension of forced oscillation testing to the development of Bode plots has also been offered. This chapter presents the governing equations which will be used to analyze and validate forced oscillation testing as a useful tool in the testing of rotary wing MAVs.

The following chapter will detail the experimental setup currently being used to perform forced oscillation tests. The capabilities of this setup stem directly from the experimental measurements needed to utilize the equations presented above.

Chapter 4: Forced Oscillation Testing: Experimental Setup

4.1 Introduction

In order for the test setup to be able to collect meaningful measurements it must satisfy several requirements. These requirements are primarily imposed by the theoretical development outlined in chapter 3.

- Sinusoidal velocity perturbation along the vehicle's X-axis
- Variable oscillation frequency and amplitude
- Dynamic measurement of X-force and pitching moment
- Real-time measurement of vehicle position
- Synchronized acquisition of force and position data

The current test setup consists of a scotch yoke mechanism capable of producing precise sinusoidal oscillations of variable amplitude and frequency. A strain gauge force balance is used to measure X-force and pitching moment. A linear position sensor is utilized to record the position of the vehicle. The signals from both the force balance and the linear position sensor are recorded simultaneously using a digital data acquisition system. The current test setup is shown in figures 4.1 and 4.2.

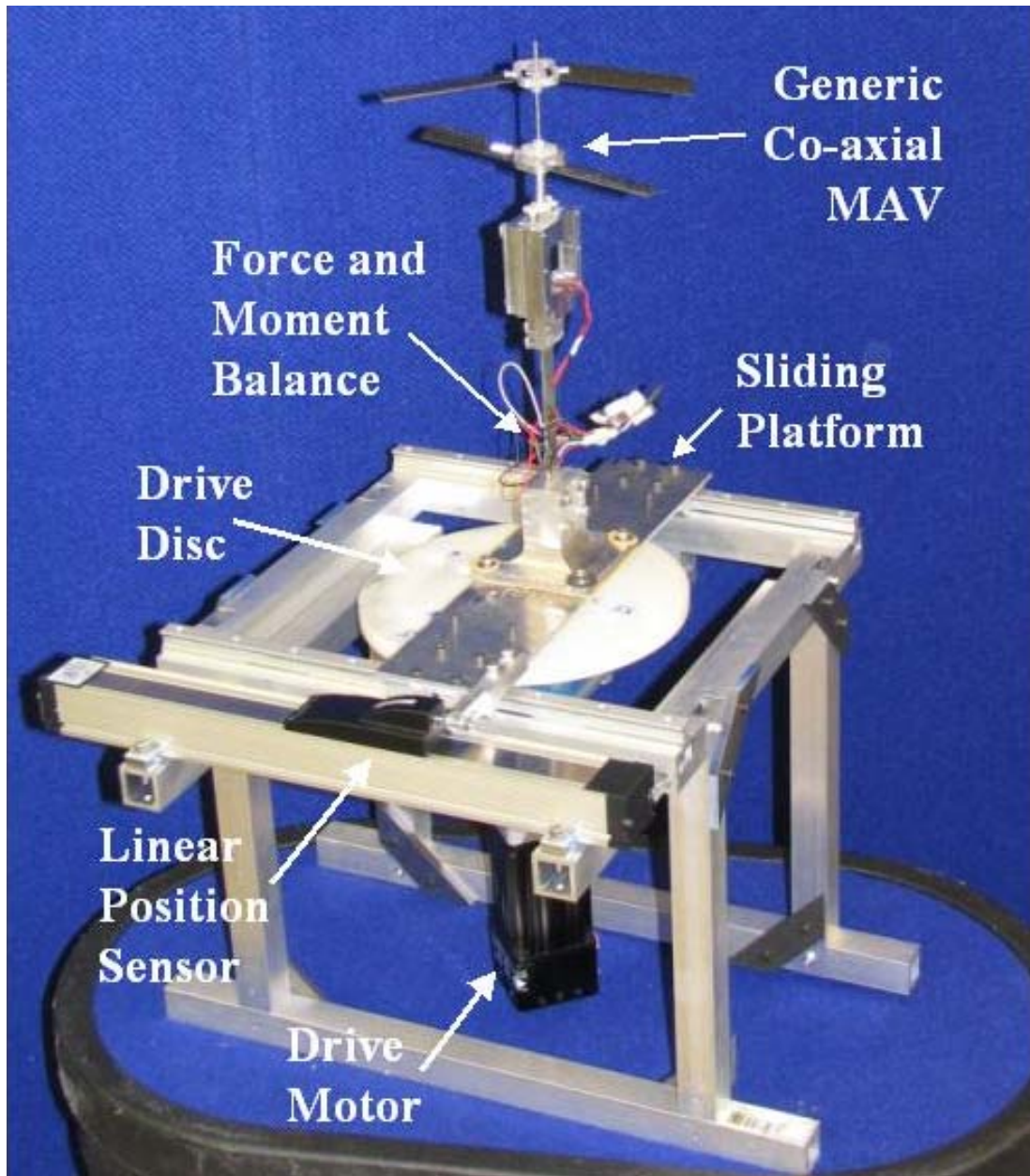


Figure 4.1 Forced Oscillation Test Stand



Figure 4.2 Data Acquisition System

The current setup is capable of producing forced sinusoidal oscillations at frequencies between 0 and 3 Hz. The amplitude of forced oscillation is variable from .75 to 3.5 inches in 1/4 inch increments. The specified forced sinusoidal oscillation as defined by the tolerances of the setup is accurate to within 0.03% in amplitude and frequency.

4.2 Scotch Yoke Mechanism

The scotch yoke mechanism consists of a rotating drive disk which induces a pure sinusoidal motion to a sliding platform by means of a pin protruding from the disc. This pin extends into a horizontal slot in the platform. A simple scotch yoke mechanism similar to the one utilized in the forced oscillation test stand is shown in figure 4.3.

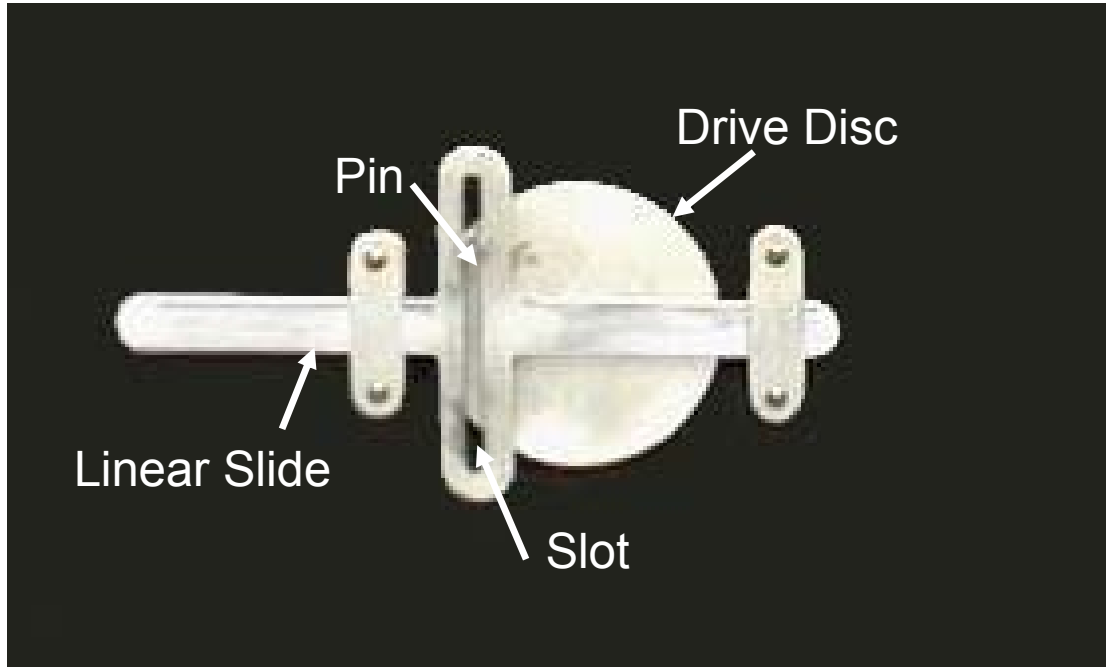


Figure 4.3 Scotch Yoke Mechanism

The scotch yoke mechanism implemented on the test stand utilizes an 8 inch diameter drive disc made of Delrin. There are holes drilled in the disc at half inch increments such that the position of the pin can be easily changed to select the amplitude of the sinusoidal motion. The disc is supported and allowed to rotate by a 1 inch flange bearing which is mounted to the test stand frame. The output shaft from the drive motor assembly passes through the bearing and is press fit to the drive disc. The motor assembly is also bolted directly to the test stand frame. The sliding platform is attached to the test stand frame by means of two Versa-Mount needle bearing guide blocks. These guide blocks are mounted on parallel 12 mm width slide rails designed specifically for the guide blocks. These slides constrain the platform to linear movement along the X-body axis of the subject vehicle. The test stand frame is constructed of interlocking one inch square aluminum tubing. Additional support has

been added to the frame structure in the form of one inch aluminum angle braces attached at each joint.

4.3 Drive Motor Assembly

The drive motor assembly consists of an Animatics SmartMotor SM2340D paired with a Carson Manufacturing Model 23EP016-LB 16:1 gear ratio low backlash planetary gear box. When paired with the gearbox, the motor is capable of producing 5.28 N-m of torque and can precisely turn the drive disc at a constant rate between 0 and 280 rpm when no load is applied. This corresponds to output frequencies of up to 4.7 Hz. When attached to the scotch yoke mechanism, the motor has shown the capability of maintaining a constant forcing frequency of up to 3 Hz. The drive motor is controlled by a desktop computer running SmartMotor Interface version 2B105. Using a 2000 per revolution encoder feedback, the motor software is capable of holding the motor rpm at a constant rate to within .1%. This software package is also capable of controlling more sophisticated motor commands, but for the initial test stand applications only constant velocity commands are required.

4.4 Force Balance

A two-degree of freedom strain gauge force balance, shown in figure 4.4 is mounted on the sliding platform. This force balance consists of a cantilevered steel beam with two full bridge strain gauge arrays mounted to the beam. The steel beam has a rectangular cross section of .125 by .5 inches. This cross section has been reduced to .07 by .5 inches at the location of the upper strain gauge array to induce an increased strain level at that location. The strain gauge arrays consist of 4 Measurements

Group, Inc. CEA-13-125UW-35 resistive strain gauges, all of which are mounted parallel to the beam such that optimal sensitivity is achieved for bending strain. The upper and lower strain gauge arrays are located at .25 and 2.75 inches from the cantilevered base of the beam respectively. Because the distance between the arrays is known, the signals from the two arrays can be used to calculate the force and moment acting at the tip of the beam. These measurements correspond to the force along the X-body axis and the pitching moment for the vehicle being studied. The total distance from the clamped end to the tip of the steel beam is 4.75 inches. The vehicle under consideration is mounted at the tip of the beam using a rigid aluminum clamp. Because the deflections of the beam during testing are very small, less than 0.1 mm, the assumption is made that the precise sinusoidal motion of the slide platform is perfectly transferred to the vehicle during testing.

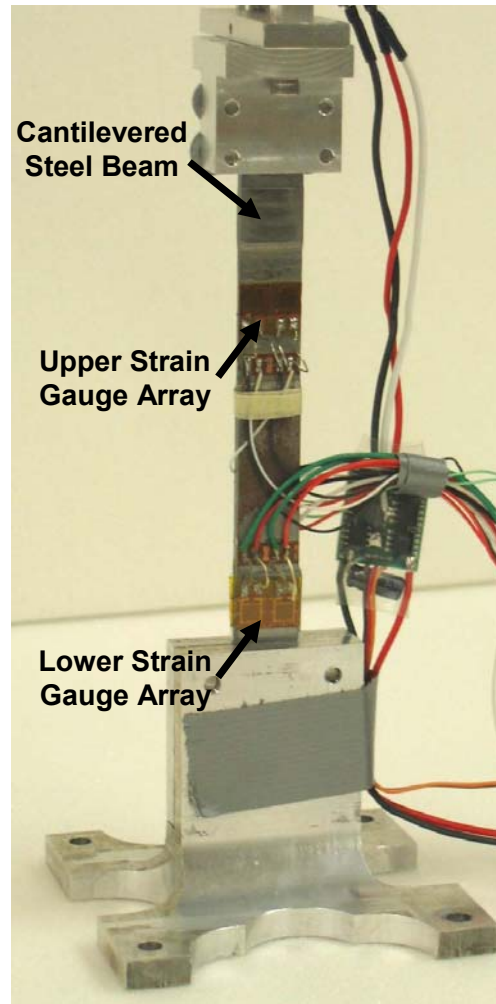


Figure 4.4 Force and Moment Balance

4.5 Signal Conditioner

The strain gauges are excited and the signal from them is amplified using a Vishay Measurements Group 2311 signal-conditioning amplifier. This amplifier is capable of exciting the strain gauge arrays with between .7 and 15 volts, and the value of signal amplification can be set between 1 and 11,000. The signal conditioner also has an analog low pass filter which can be set between 10 and 10,000 Hz in increments of power ten. Because the response of the vehicle which is being tested occurs at the

frequency of forced oscillation the low pass filter is used to reduce the high frequency noise present in the unfiltered signals from the strain gauges. The cutoff frequency of this analog filter was set to 1000 Hz, as that was found to be the lowest filter setting which would not introduce any noticeable phase delay at the forcing frequency. The strain gauges are excited using the 10 volt excitation setting on the signal conditioner. The gain of the amplifier was chosen to be 5000. This value was selected to give the highest gain possible without causing unnecessary amplification of noise in the signal. Because the aerodynamic component of the force signal is very small the largest feasible gain was selected so that the signal could be more easily measured. The gain value of 5000 was chosen by running several test cases with different gain settings and comparing the standard deviation of the first term Fourier series representation between subsequent tests. A plot of this investigation is shown in figure 4.5. From the figure a gain value of 5000 was selected as the largest gain without inducing a significant increase in the standard deviation of the results.

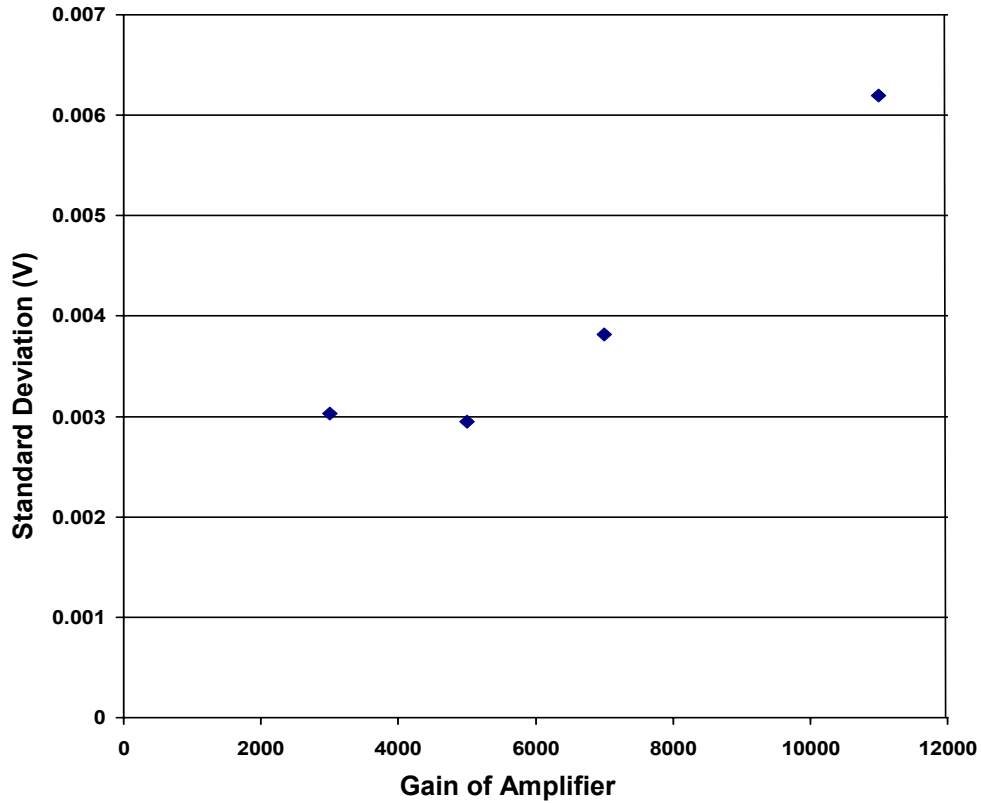


Figure 4.5 Investigation of Optimal Amplifier Gain Setting

4.6 Position Sensor

In order to properly analyze the results of a forced oscillation test, the aerodynamic response data must be time synchronized with the forced perturbation. For this reason a linear position sensor is used to record the position of the linear slide during testing. A Novotechnik TLH series linear position transducer with a 225 millimeter stroke is mounted parallel to the guide rails of the linear slide and is rigidly connected to the sliding platform. This position sensor is excited by a computer power supply which produces a constant 12 volt excitation.

4.7 Data Acquisition System

The two signals from the conditioned strain gauge outputs as well as the signal from the linear position sensor are fed into the data acquisition box via BNC cables. The box is a National Instruments NI-SC-2435 connector block which utilizes SCC-FT01 modules for all three signals. The output of the data acquisition box is fed into a Alienware laptop computer via a National Instruments DAQCard-6062E PC card. The analog data from the data acquisition box is digitally recorded using MATLAB. MATLAB utilizes a modified version of the program “mavdaq”, originally written by Aubrey Goodman to record the test data to a specified file location. This program specifies the input channels, the sample rate, the length of the test and the file name under which to save to recorded data. By recording the signals from the strain gauge arrays as well as the signal from the linear position sensor simultaneously, the resulting data contains a position signal that is time synchronized with the force signal. This is of fundamental importance when performing data reduction in order to properly separate the stability derivatives from the force signals.

4.8 Rotor Systems Under Consideration

Three rotor systems have been considered in the initial analysis of the forced oscillation test stand. These rotor systems are a generic co-axial rotor system modeled after MICOR, an 11 inch diameter teetering rotor and an 11 inch diameter rotor with a rigid hub. Each of these rotor systems were chosen to validate the test process for a specific reason. The generic co-axial rotor system was chosen as a representative of the type of rotor system currently in use on the most advanced rotary

wing MAV currently being developed at the University of Maryland. The 11 inch diameter teetering rotor is also representative of the vehicles currently under development. It was specifically chosen because of the simpler design and greater thrust produced when compared to the co-axial rotor system. The response of this rotor will therefore be more easily measured. A clearly measurable response is of course a desirable trait for the current research goals. The rigid hub rotor was chosen as an example of a rotor which is capable of imparting a pitching moment response to the rotor shaft. This capability was necessary in order to show the ability of the current test stand to measure both the X-force and pitching moment response of a vehicle. The design and specifications of each of these rotor systems is given in the subsections below.

4.8.1 Generic Co-axial

The original rotor system tested was a generic co-axial MAV rotor system modeled after the University of Maryland's co-axial rotary wing MAV, MICOR [2], [3]. This system consists of two Astro Flight Firefly coreless motors with integrated 4:1 planetary gearboxes. These motors drive two counter rotating 7.25 diameter freely teetering rotors. These rotors utilize cambered rectangular planform carbon fiber blades with a chord of .615 inches. The rotor separation is 2 inches and both rotors are set to a fixed collective pitch angle. The upper rotor blades are set at 8 degrees collective pitch and the lower rotors are set at 12 degrees. The speed of the rotors is controlled by using a variable voltage Sorensen HDP 15-20 DC power supply. At normal operating conditions the tip Reynolds number for this rotor system is approximately 23,000. Figure 4.6 depicts the generic co-axial rotor system.

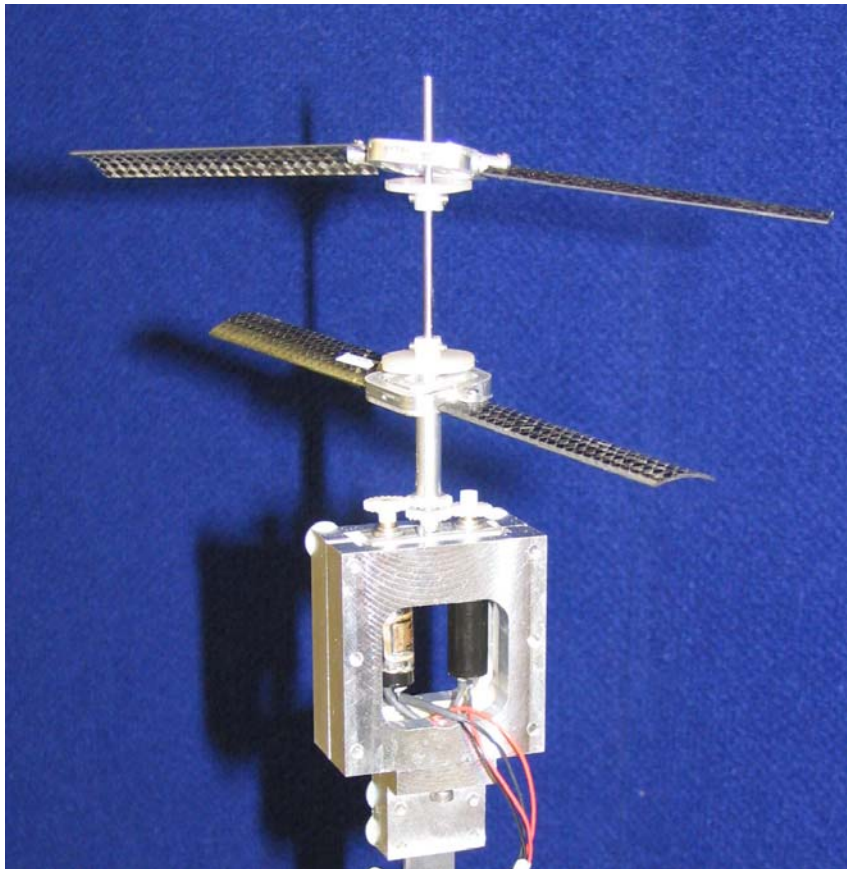


Figure 4.6 Generic Co-axial Rotor System

4.8.2 Teetering

The second rotor system to be tested consists of a simple single main rotor. This rotor system is portrayed in figure 4.7. The rotor is powered directly by an AXI 2204 Outrunner brushless motor. This rotor has an overall diameter of 11 inches, and utilizes twisted cambered aluminum blades with a chord of .787 inches. The blades have a fixed collective pitch of 16 degrees with -8 degrees of twist over the span of the blades. The rotor is freely teetering, meaning that both blades are constrained to the same flapping angle, and the flapping hinge is not offset from the rotor shaft. The

rotor hub is connected directly to the output shaft of the motor via a steel collar. The motor is powered by a 12 volt constant voltage computer power supply. The motor is controlled by a GWS STII Microprocessor Controlled Servo Tester, which provides a pulse output to the Castle Creations Phoenix-10 Brushless Speed Controller. The motor speed is set by adjusting the servo tester to the desired setting. At standard operating conditions the tip Reynolds number for this rotor system is approximately 47,000.



Figure 4.7 Single Teetering Rotor

4.8.3 Rigid Hub

The 11 inch diameter rigid rotor has identical properties to those listed for the teetering rotor. The rigid configuration of this rotor is achieved by attaching a small aluminum plate to the top of the rotor hub. This aluminum plate prevents any rotation about the flapping hinge and effectively transforms the teetering rotor into a rigid

hub. Because this rotor system has no flapping hinge, the rotor is capable of inducing a pitching moment to the rotor shaft.

4.9 Description of Blade Flapping Motion

As described above, the current test stand is designed to produce a linear sinusoidal perturbation in the velocity of a test vehicle along the vehicle's X-axis. Because of the nature of MAVs, the dynamic characteristics are dominated by the rotor response. For that reason the current research focuses primarily on the response of the rotor systems to the perturbation induced by the forced oscillation motion. The perturbation in velocity along the X-axis of the test vehicle was chosen because it induces one of the primary aerodynamic responses for a rotary wing vehicle. When a perturbation in the forward velocity of the vehicle occurs, it causes the rotor blade on the advancing side of the rotor disc to see an increase in relative velocity. Similarly, the blade on the retreating half of the rotor disc sees a reduction in relative velocity. This differential change in relative velocity causes increased lift over the advancing half of the rotor plane and decreased lift over the retreating portion. This dissymmetry in lift causes the advancing blade to flap up and the retreating blade to flap down. For a teetering rotor this flapping response acts 90 degrees out of phase with the variation in lift. This 90 degree phase delay is such that an increase in forward velocity will cause the rotor blades to reach their maximum flapping angle over the front of the vehicle and a minimum angle over the rear. This blade flapping response effectively causes a tilt back of the rotor plane away from the perturbation as shown in figure 4.8.

Perturbation in Forward Velocity

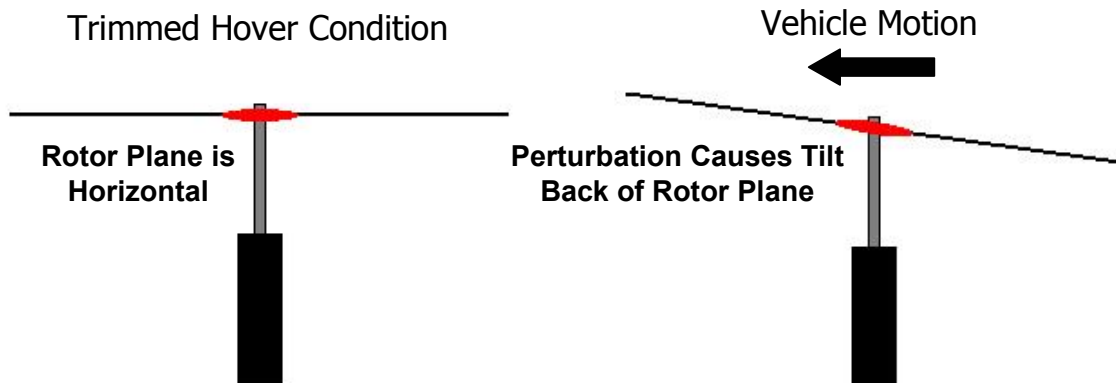


Figure 4.8 Blade Flapping Response to Perturbation in Forward Velocity

The flapping response of the rotor to the perturbation in forward velocity changes the orientation of the tip path plane of the rotor. For flight near hover conditions and for small changes in the orientation of the rotor plane the thrust vector produced by the rotor acts perpendicular to the rotor plane. For this reason a change in the tilt of the rotor plane effectively changes the orientation of the thrust vector produced by the rotor. Because there is now a component of the thrust vector acting along the X-axis of the vehicle, the perturbation in forward velocity has caused an aerodynamic force reaction in the X-direction. Although a teetering rotor is not capable of exerting a pitching moment to the rotor shaft itself, if the vehicle as a whole is being considered, the offset of the rotor forces from the center of gravity of the vehicle will also cause a pitching moment. The X-force and pitching moment reaction to a perturbation in forward velocity are depicted in figure 4.9.

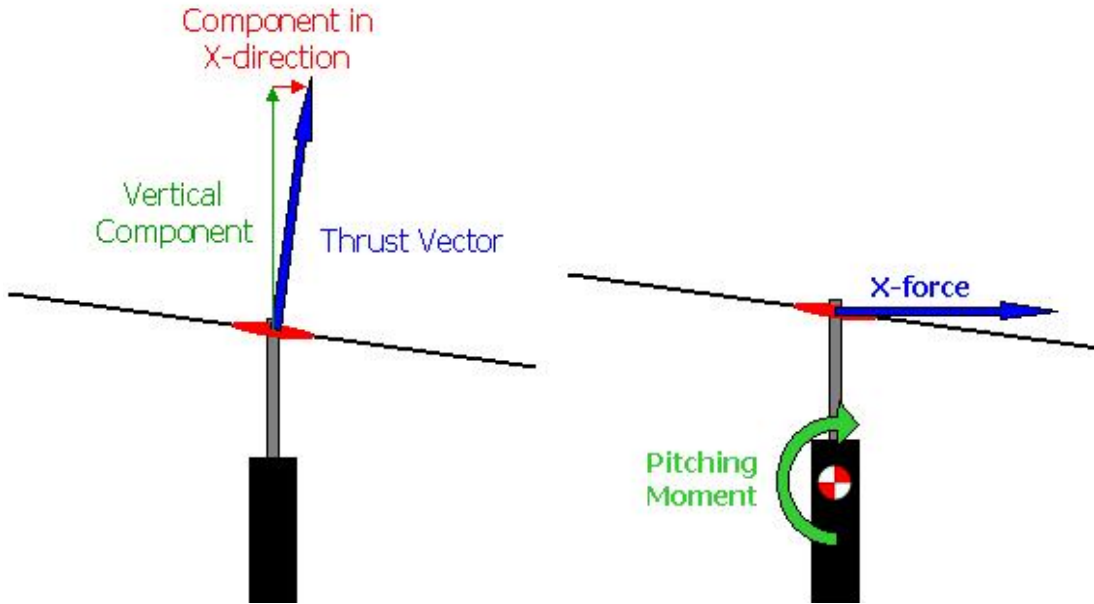


Figure 4.9 X-Force and Pitching Moment Response

For a perturbation in forward velocity near hover there is also an off axis flapping response of the rotor. This additional rotor response is discussed in more detail by Padfield [38]. Because of non-uniform inflow effects caused by perturbations in velocity near hover the lateral flapping response can often be on the same order of magnitude as the expected longitudinal flapping response described above. This off axis response is not measured by the current test stand. The measurement of the longitudinal flapping response is not corrupted however by the lateral flapping component. The current force balance has been designed to be insensitive to the force produced by the off-axis flapping and thus only measures the X-force response caused by longitudinal flapping.

It should be noted that for the initial research entire vehicles were not tested. As a simplified case to vehicle testing, representative rotor systems were tested. For

this reason the pitching moment response of the teetering rotor systems was not considered. For non-teetering rotor systems however, it is possible for the rotor to exert a moment to the rotor shaft. The rigid rotor described in sub-section 8.3 of this chapter is such a system. For the rigid hub, the pitching moment response was measured as a means of demonstrating that the current force balance is capable of measuring both the X-force and the pitching moment response of the test rotor systems.

4.10 Chapter Summary

In summary, a test stand and the accompanying hardware has been developed and implemented. This test stand is capable of producing the necessary motion needed to perform forced oscillation testing of a rotary wing MAV. The necessary sensors and data acquisition hardware have also been integrated into the test setup, such that the required measurements can be recorded. Three rotor systems which are representative of rotary wing MAVs have also been fabricated for use in initial testing of the forced oscillation technique. Additionally, the flapping response characteristics of a teetering rotor have been presented. This flapping response generates the X-force reaction to perturbations which the current test setup has been designed to measure.

The next chapter presents the test procedure required to acquire a measurement of the stability parameters of a rotary wing MAV.

Chapter 5: Forced Oscillation Testing: Test Procedure and Data Reduction

5.1 Introduction

The standard forced oscillation test procedure consists of several steps. These steps are outlined below and then discussed in more detail within the following sections. The result of one set of tests is the measurement of the force and moment response of the test vehicle at a specific forcing frequency. This measurement gives either the value of the two corresponding stability derivatives of the vehicle, or one gain and phase point on each of the vehicle's respective Bode plots. The representation of this data is considered as an additional step to those outlined below and is summarized in the final section of the chapter. The steps taken in the execution of a forced oscillation test are as follows.

- Choose forcing frequency and amplitude
- Determine the proper speed setting for the drive motor based on desired forcing frequency
- Choose applicable sample rate based on input channels and forcing frequency
- Determine length of test and proper name for data file
- Run tare tests
- Run rotors-on tests
- Perform data reduction

From the outline of the test procedure it is clear that two types of test are needed to determine the stability parameters at each combination of test conditions. These two tests are a tare test and a rotors-on test. The need for the two tests arises from the fact that the final result is calculated from purely the aerodynamic reaction of the rotor system. In order to separate the aerodynamic response from the inertia forces created by the oscillation motion the results of the tare test are subtracted from those for the rotors-on test. This subtraction of inertia forces produces a measurement of the purely aerodynamic reaction of the rotor to the induced perturbation.

5.2 Setup of Test Parameters

Before an actual test can be run, the parameters which govern the test conditions must be chosen. The methodology of determining each parameter is discussed in the following subsections. The subsections are organized in such a manner as to follow the logical sequence of steps as the user would follow in preparation for testing. The testing parameters which must be determined before testing are listed below.

- Forcing frequency
- Amplitude of forced oscillation
- Drive motor setting
- Sampling rate
- File name for saved test data

5.2.1 Forcing Frequency

The first step in the test procedure is choosing the forcing frequency at which the test will be run. In order to perform a stability derivative analysis, the frequency chosen

is not significant so long as it is within the linear response range for the vehicle. For Bode plot type analysis data is taken at incremental frequencies over the range of interest. Each point on the Bode plot represents one forcing frequency. The choice of forcing frequency drives all of the remaining test parameters so it is the first thing to consider. The next consideration is the amplitude of the force oscillation. For most tests the largest available amplitude is chosen, i.e. 3.5 inches. Smaller amplitude may be appropriate however for high frequency testing if the inertia loads caused by testing at large amplitudes are so large that they saturate the output of the signal conditioner. The oscillation amplitude generally used for different forcing frequencies is depicted in table 5.1. The appropriate oscillation amplitude for each frequency range was determined experimentally by selecting the amplitude that would cause the largest rotor response without saturating the signal conditioner.

Forcing Frequency (Hz)	Oscillation Amplitude (in)
.4 – 1.2	3.5
1.3 – 1.6	2.5
1.7 – 2	2
2.1 – 2.2	1.5
2.3 – 2.5	1

Table 5.1 Oscillation Amplitude Setting

5.2.2 Drive Motor Setting

Once the proper frequency has been chosen and the test stand has been set to produce the desired amplitude of forced oscillation, the next step is to determine the proper

drive motor setting. The drive motor is controlled by the motor control software. This software transmits a program to the motor which sets the constant rotational rate produced at the output shaft of the gearbox. In order to set the motor to the proper rotational rate, the velocity input to the program must be changed to the proper value. This value is determined by multiplying the desired frequency at the output shaft by 522066. For quick reference table 5.2 was created which gives the motor settings over the applicable frequency range.

Frequency (Hz)	Motor Setting
0.2	104413
0.3	156620
0.4	208826
0.5	261033
0.6	313240
0.7	365446
0.8	417653
0.9	469859
1	522066
1.1	574273
1.2	626479
1.3	678686
1.4	730892
1.5	783099
1.6	835306
1.7	887512
1.8	939719
1.9	991925
2	1044132
2.1	1096339
2.2	1148545
2.3	1200759
2.4	1252958
2.5	1305165

Table 5.2 Motor Setting to Achieve Desired Forcing Frequency

5.2.3 Sampling Rate

The next step in the test process is to determine the sampling rate for the data acquisition program. Because of the methodology use during data reduction, each oscillation during testing must be recorded by a specific number of samples. In other words, the number of samples which define one complete oscillation must be an

integer value. The reasoning for this restriction will become clear in the description of the data reduction process. The second restriction placed on the sample rate is the limited ability of the data acquisition system to acquire data. For a standard test with the current setup there are three input channels, namely the two signals from the strain gauge arrays and the signal from the linear position sensor. It was found that with these three channels as the inputs the data acquisition system is capable of acquiring data at just over 800 samples per second. If another channel is added, the capability is reduced to just over 600 samples per second. Because of the dynamic nature of the testing and the presence of high frequency noise in the measurements, it is desirable for the sample rate to be as close to the maximum value as possible. To satisfy the first constraint, the sample rate divided by the forcing frequency must be an integer. The second constraint is satisfied by choosing the sample rate closest to either 600 or 800 samples per second which satisfies the first condition. Table 5.3 lists the sample rates used for each forcing frequency.

Frequency (Hz)	Sample Rate (3 channels)	Sample Rate (4 channels)
0.2	800	600
0.3	801	600
0.4	800	600
0.5	800	600
0.6	801	600
0.7	805	602
0.8	800	600
0.9	801	603
1	800	600
1.1	803	605
1.2	804	600
1.3	806	611
1.4	805	609
1.5	801	600
1.6	800	600
1.7	816	612
1.8	801	603
1.9	817	608
2	800	600
2.1	819	609
2.2	803	605
2.3	805	621
2.4	804	600
2.5	800	600

Table 5.3 Proper Sample Rate for Each Forcing Frequency

5.2.4 File Organization

Once the sample rate and motor setting are determined, the length of the test is chosen. The standard length of a test is 180 seconds. Other lengths may be used, but from analysis of test results it was determined that 180 seconds provides sufficient data without generating excessively large data files. From this information an

appropriate name for the data file corresponding to the current test can be created. This file name completes the necessary inputs to the data acquisition code, “mavdaq.”

For simplicity in organizing the resulting test data, and to maintain consistency throughout data reduction, the data files are named as follows. The first few characters give a general description of the test case. For instance “single_teetering” may be used to indicate the test of a single freely teetering main rotor. The next few characters indicate the forcing frequency, oscillation amplitude and sampling rate. For example, “14Hz_35in_609ps” would indicate a forcing frequency of 1.4 Hz, oscillation amplitude of 3.5 inches, and sampling rate of 609 samples per second. The final part of the name consists of which instance in the test series this set of data represents and the rotor conditions. As an example, “tare4” would indicate the fourth tare test in the test series. Similarly, “124_3” would indicate the third rotors-on test, where the rotor rpm was controlled by setting the servo motor controller to 124. It is important that the last character of the file name is an integer indicating which test in a series of similar tests the data in the corresponding file represents. The reasoning for this numbering scheme will become clear in the explanation of the data reduction methodology. Combining each of the above inputs, an example file name would be “single_teetering_14Hz_35in_609ps_tare4.”

5.3 Tare Testing

Now that all of the necessary parameters have been determined, the inertia measurements from the tare tests can be collected. For these tests the rotor is stationary and held in place by a small piece of tape. This is done so that motions of

the non-spinning rotor do not corrupt the measurements. Because the mass of the tape is very small, its contribution to the inertia measurements is considered negligible. At this point, the drive motor is turned on, which starts the forced oscillation motion. The corresponding signals from the strain gauge arrays and linear position sensor are recorded using the program “mavdaq” via MATLAB. The inputs to this program are the input channels corresponding to the data signals, the sample rate, the length of the test in seconds, and the corresponding file name under which the data will be saved. This procedure is then repeated until a sufficient number of tests have been recorded to determine the inertia forces caused by the forced oscillation.

5.4 Rotors-on Testing

Once the tare tests have been concluded, aerodynamic response data can be collected from the rotors-on tests. A similar procedure to that used in running the tare tests is followed. The only modification is that the rotor system under investigation is set to the desired operating conditions before starting the forced oscillation. For the generic co-axial MAV, setting the rotor conditions is done by adjusting the voltage on the variable power supply to the desired level. For the case of the single main rotor, the rotor speed is set by adjusting the servo tester to the desired setting, as indicated by the digital output on the front of the tester. Once the rotor conditions have been set, the same procedure as used for the tare test is executed until sufficient data has been collected to determine the aerodynamic response of the rotor.

5.5 Data Reduction

The final process in the test procedure is reduction of the raw data into useful values. This is done with the aid of MATLAB and the implementation of two computer codes written specifically for this application. The primary concept behind the data reduction is to take all of the available test data for each test case and reduce it to one oscillation worth of averaged data for both the tare test and the rotors-on test. This data is then used to compute either the applicable stability derivatives for that test case or points on a Bode plot corresponding to the given forcing frequency. The correlation between the forced velocity perturbation and the resulting aerodynamic force reaction is also calculated as a means of evaluating the linearity of the relationship between the rotor reaction and the perturbation.

5.5.1 Use of MATLAB Program “mavplotDZ”

The first step in the data reduction process is the processing of the raw data by “mavplotDZ.” This program is used as a function within the second program “mavavD,” but its use is more fundamental so it will be discussed first. First, “mavplotDZ” loads two of the saved data files. The first data file is a tare test and the second is a corresponding rotors-on test. The inputs to the program are the names of the two files, and the length and sample rate of each. The program processes each of the two files in exactly the same manner. The data reduction process will only be explained for one of the two files even though in actuality it is being carried out twice simultaneously. Once the files are loaded, “mavplotDZ” calculates the length of one oscillation from the forcing frequency and the sample rate. The data is now divided into sections, each of which is the length of one oscillation. These sections are then

averaged together to give one oscillation worth of averaged data as shown in figure 5.1. This process is more commonly known as synchronous averaging. By performing this average over a long test run, much of the random noise is removed from the signal.

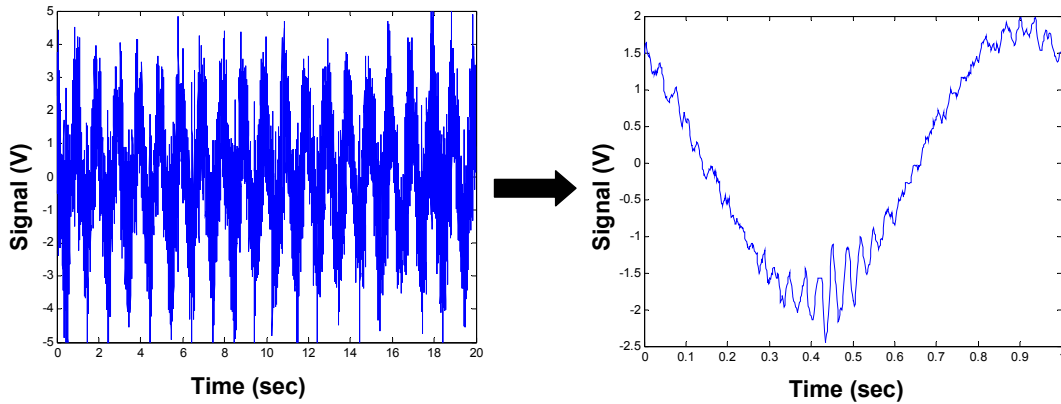


Figure 5.1 Synchronous Averaging of Output Signal

The signal from the linear position sensor is now used to shift the data. This is done such that the single oscillation worth of data starts at the beginning of one forced oscillation, i.e. when $x(t) = 0$. The function $x(t)$ indicates the position of the slide platform with respect to time. The single oscillation of data ends one data point before $x(t)$ returns to zero. This shift is performed by setting a checkpoint near the mean value of the position signal. Next, “mavplotDZ” finds a point in time when the position signal crosses from above the checkpoint to below it. Then a second point is determined which corresponds to the next point in time when the position signal crossed from below the checkpoint to above it. The average of these two points in time gives the point in time which corresponds to the minimum value of the

sinusoidal position signal. Using this time of minimum position, all of the signals are shifted backwards in time one quarter of the oscillation period. This corresponds to aligning the signals such that the first data point in the single oscillation of data occurs when $x(t) = 0$. This shift of the signal with respect to time is depicted in figure 5.2.

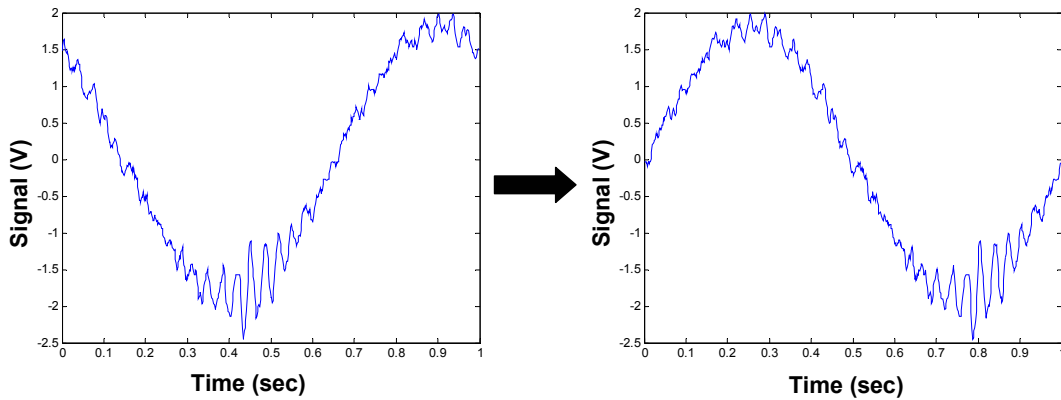


Figure 5.2 Time Shift of Output Signal

The discrete Fourier transform of each signal is now taken in order to determine the coefficients of the Fourier series approximation of the signal. The use of the discrete Fourier transform and its applications is discussed in more detail by Ramirez [39]. The first term of the Fourier series approximation is set to zero in order to remove the DC component of each signal. At this time higher harmonic components can also be removed. This process is equivalent to a digital low pass filter. Because the analog low pas filter was limited to relatively high frequencies, above 1000 Hz, the data is generally filtered at 20 Hz at this time unless higher frequency noise is desired for some type of special analysis. The use of the discrete Fourier transform to digitally

filter the output signal is depicted in figure 5.3. At this time “mavplotDZ” is capable of subtracting the tare case from the rotors-on case to determine the aerodynamic response. This is generally not done however. For most cases it is more systematic to average whole set of test together using “mavavD” before subtracting the tare test.

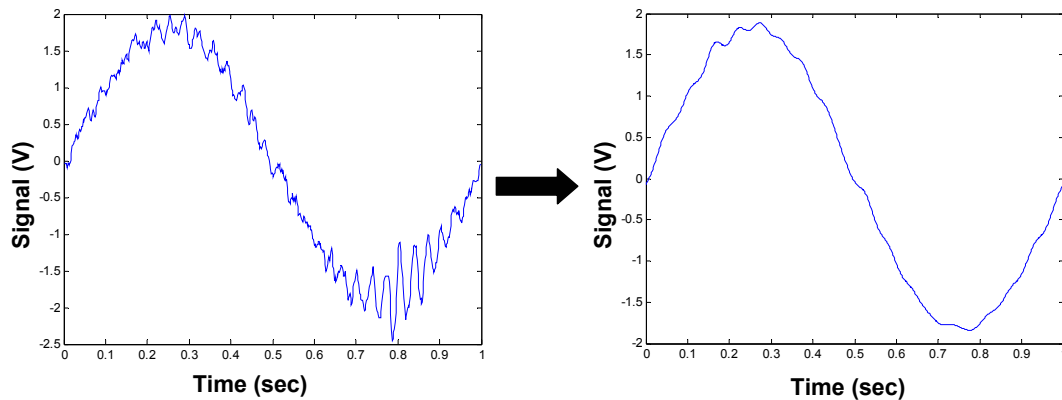


Figure 5.3 Filtered Output Signal

5.5.2 Use of MATLAB Program “mavavD”

In order to process multiple tests for each frequency at once, the MATLAB program “mavavD” is employed. This program cycles through set of tests taken for a certain condition. The program then averages the results of “mavplotDZ” for these tests to give one result for the whole set of tests. This process is depicted in figure 5.4. Once the results have been averaged “mavavD” uses these averaged results to determine either the appropriate stability derivative or the relevant points on a Bode plot. This is done by first subtracting the tare case from the rotors-on case. This subtraction is performed to remove the inertia contributions to the signal. Removing the inertia contribution leaves the average aerodynamic response from all of the tests at the

specified conditions. This process is portrayed in figure 5.5. The finite Fourier transform of the aerodynamic response is taken to determine the coefficients of the Fourier series approximation of the signal. For calculation of both the stability derivatives and the points on the corresponding Bode plot, the higher harmonic terms of the Fourier series are dropped, as only the first harmonic term is of interest. The first term approximation of a representative signal is shown in figure 5.6.

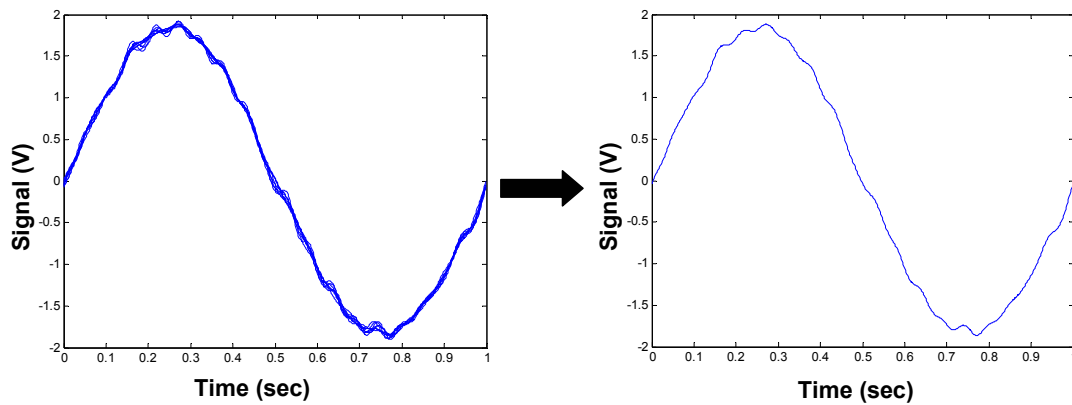


Figure 5.4 Averaging of Multiple Tests

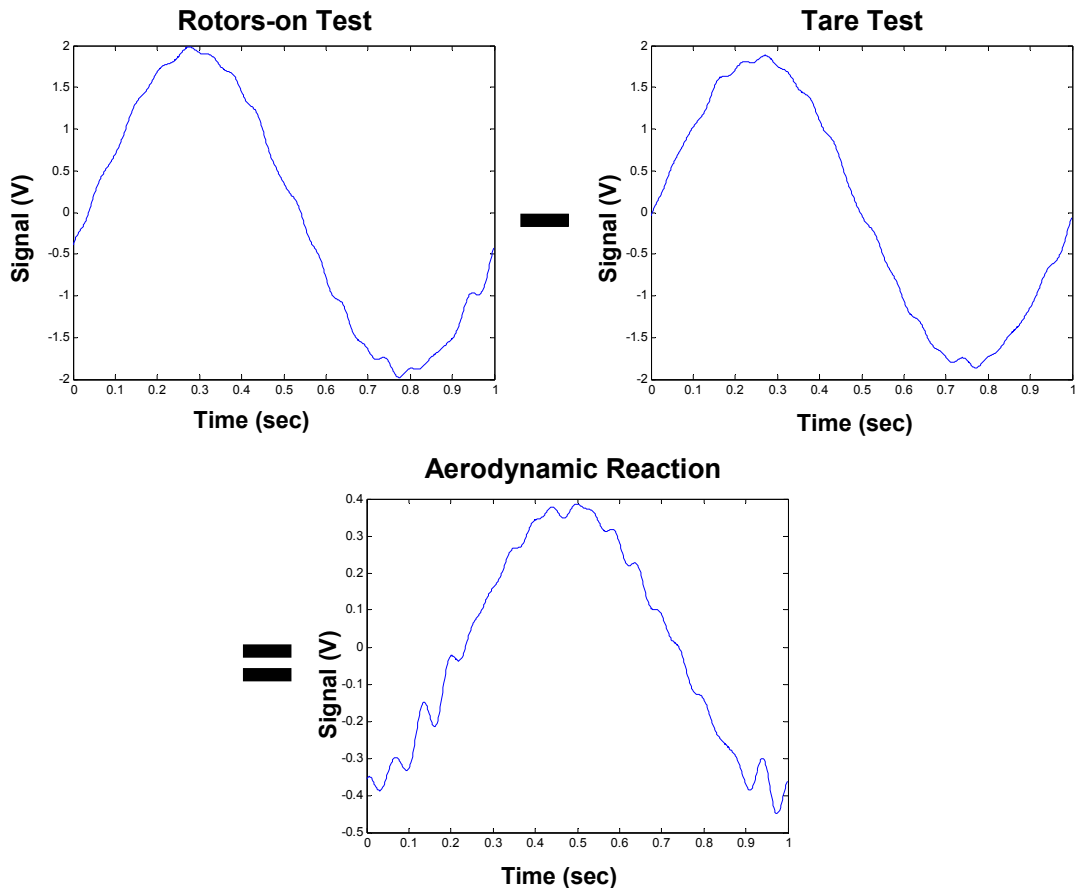


Figure 5.5 Subtraction of Tare Test from Rotors-on Test

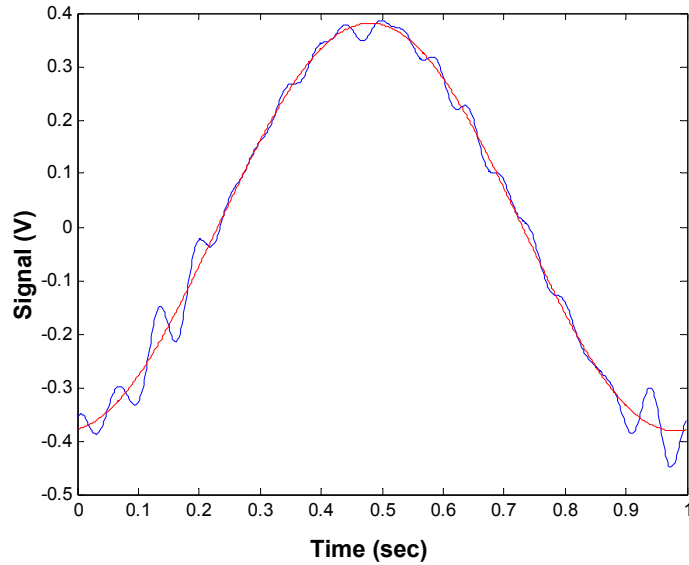


Figure 5.6 First Term Fourier Series Approximation of Signal

The calibration matrix of the force balance is now applied to convert the signal from volts to Newtons and Newton-meters. Recognizing the sine component of the first harmonic term as F_{OUT} and the cosine component as F_{IN} , equations 3.13 and 3.14 can be applied to deliver the appropriate results. These results are returned as the output of “mavavD.”

The program “mavavD” is also used to compute the correlation between the forced velocity perturbation and the aerodynamic force response of the vehicle. The correlation between the two signals gives a measure of the linear relationship between the input velocity perturbation and the output force response, as discussed by Bendat and Piersol [40], [41]. This is similar to calculating the coherence for flight test data. Because the input is a simple sinusoid rather than a frequency sweep as in a standard flight test, the coherence of the two signals is nearly one for all cases and thus does not lend much insight into the dependence of the output on the input. The correlation

of the two measurements is not a function of frequency, rather it considers the signal as a whole and is thus much more useful for the case when only one forcing frequency is present. Unlike coherence however, a phase delay in the system can cause the correlation to be less than one, even if the system is linearly dependent. For this reason, the phase delay in the force response must be removed before calculating the correlation of the two signals. Once the correlation has been calculated it is also returned as an output of “mavavD”

The final function of “mavavD” is to provide a visual check of the test data. The program plots the results from “mavplotDZ” for each of the tests in the set of tests at those conditions. An example of this plot can be seen in figure 5.7. From this type of plot it is easy to spot any individual tests which do not appear similar to the other tests in the set. Rather than allowing these tests to be averaged in with the other data and possibly corrupting the results, they can be isolated from the group and analyzed individually to determine the cause of the errant results. This technique can be used to spot an unexpected change in the test conditions or a failure in the equipment. This step justifies the procedure of taking multiple tests for each test condition. The same amount of data could be collected by running a single longer duration test, but if there was an error during testing there would be no way to tell until long after the tests were taken. By taking several shorter duration tests the identification of peculiarities during testing is made much simpler.

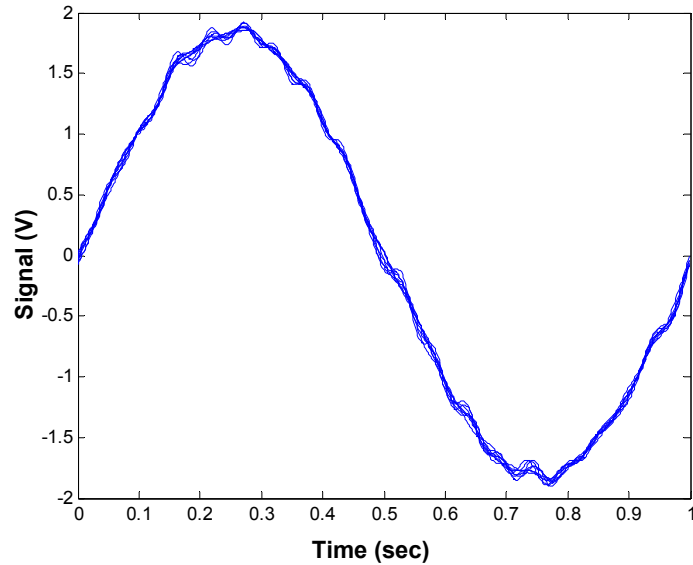


Figure 5.7 Simultaneous Presentation of Multiple Tests

5.6 Presentation of Results

The final step in the test process is the presentation of the resulting data. There are essentially three types of data that can be presented. The first data type is the stability derivatives resulting from a single set of test conditions. The second method of representing the data is by construction of a Bode plot from a series of tests over several forcing frequencies. The final piece of information which can be presented is the correlation between the input perturbation and the output rotor response. Each of these representations of the test results are discussed in more detail in the sub-sections that follow.

5.6.1 Stability Derivative Representation

The presentation of a stability derivative measurement is by far the most basic way of portraying the result of a forced oscillation test. A stability derivative can be

determined from a single set of tests rather than needing tests over a large frequency range to portray the results such as is required for Bode plot representation. The stability derivative measured from a set of tests is simply presented as a value as defined by equations 3.16 and 3.17.

5.6.2 Bode Plot Representation

The representation of test data in Bode plot form is much more complicated than the stability derivative representation of a single test. The relevant background information on the construction and use of Bode plots can be found in Roskam [42]. The nature of a Bode plot requires the representation of the data over a large range of frequencies. In order to construct a Bode plot from forced oscillation test data, a series of tests must be performed over a range of forcing frequencies. The results of each forced oscillation test can only be used to represent the response of the vehicle at one frequency. This is indeed one of the shortcomings of forced oscillation testing. A Bode plot of the vehicle response is constructed one frequency point at a time. The data at each frequency is found by selecting the desired forcing frequency and collecting the corresponding data. That data is then converted to two points, one for the gain and one for the phase on the relevant Bode plot. The calculation of these data points is carried out by applying equations 3.26 and 3.27 to the test results.

5.6.3 Presentation of Correlation Measurements

An additional result of testing beyond the response characteristics described above is the correlation measurement. The correlation result returned from testing is a measure of the linearity of the relationship between the forced oscillation motion and

the output response of the vehicle. Additional applications of correlation measurements and the relevant theory are given by Bendat and Piersol [40], [41]. In the current setup, the correlation measurement is used as a means of evaluating the quality of the measured response data. A low correlation measurement indicates that there is significant noise in the measurement or that a non-linear region of the response has been encountered. This correlation measurement is especially useful in conjunction with Bode plot of the response. By observing the correlation of the measurements over the entire range of frequencies it is possible to note regions of the response where excessive noise or other non-linearities are present. At that time additional investigation into measurements in the non-linear range can be conducted.

5.7 Chapter Summary

In summary, this chapter details the test procedure currently used in the collection of forced oscillation test data. A step by step procedure is outlined such that the tests could be reconstructed by a user unfamiliar to the test setup. The methodology used to reduce raw test data into useable measurements is also presented. Finally, the conversion of individual results into a meaningful format is discussed.

The following chapter presents the initial testing and analysis performed using the test setup and procedure outlined in chapters 4 and 5. This analysis serves as the preliminary investigation into the currently developed forced oscillation technique as a valid method for measuring the stability parameters of a rotary wing MAV.

Chapter 6: Validation of Forced Oscillation Test Process

6.1 Introduction

The primary focus of this chapter is to discuss how the forced oscillation test setup and procedures described in chapters 4 and 5 are validated. The following discussion will detail the test data collected and the accompanying analysis. The motivation of this portion of the research is to provide a validation of the experimental technique. Observations of the experimental results are used to provide a qualitative validation based on the expected behavior of the test process. The initial approach will focus on forced oscillation testing from a stability derivative perspective. An extension of the test process to Bode plot representation will be then be discussed and the two different data representation methods will be compared. Lastly, an analytical model of blade flapping response will be used to provide a quantitative validation to support the test results.

It should be noted that for the initial analysis of the technique complete vehicles were not tested. Rather, only rotor systems which are representative of current MAV designs were examined. For most rotary wing vehicles near hover, the rotor response dominates the force and moment response to perturbations in flight condition. This is especially true for the types of MAVs which are being tested at this time because they contain little or no aerodynamic surfaces besides the rotor. For this reason, analysis of simple representative rotor systems is considered sufficient for the initial validation of the test process.

6.2 Analysis of Test Results, Stability Derivative Perspective

The first section of analysis focuses on the theory used in conjunction with traditional forced oscillation techniques used to study fixed wing aircraft. The theoretical development of this type of testing uses stability derivatives to represent the aerodynamic response of the vehicle. While this theory is not necessarily applicable to rotorcraft, as previously discussed in section 3.2, it will still serve as a base point for validation of the technique. The stability derivative X_u as determined from a forced oscillation test is given by equation 3.16 as

$$X_u = \frac{|F_c|}{A_0 \omega} \quad (6.1)$$

In equation 6.1, it should be noted at this time that X_u is not a function of A or ω , rather they are simply used to scale the magnitude of the output relative to the magnitude of the forced perturbation. For this reason, the test process should ideally produce the same value for X_u regardless of the forcing frequency or the amplitude of the forced oscillation. This concept is of course subject to several constraints, imposed both by the test setup and the theory.

6.2.1 Constraints on Evaluation of Stability Derivatives

The first constraint is a function of the equipment available to measure the aerodynamic response of the rotor. The magnitude of the velocity perturbation induced by the forced oscillation is the product of the oscillation frequency and the amplitude of the forced oscillation. The response of the rotor is in turn caused by this velocity perturbation. In order to determine the stability derivative of the rotor, the response of the rotor must be large enough to be accurately measured by the force

balance. If the combination of the forcing frequency and the amplitude of the forced oscillation is too small the response of the rotor will not be significant enough to be accurately measured. Thus, for the forced oscillation test to effectively measure the stability derivatives of the rotor system the magnitude of the velocity perturbation must be sufficiently large.

The second constraint is imposed by the theoretical assumptions made in the use of stability derivatives as a means to describe the response of the rotor to perturbations. These assumptions are that the perturbation is a small change to the trimmed flight condition and that the perturbation motion is slow with respect to the response of the rotor. For the current test setup the maximum attainable perturbation in forward velocity causes a rotor advance ratio of less than .05. This change in flight condition is within the assumption of small perturbations about hover. For this reason the more significant constraint imposed by theoretical assumptions is that the forcing frequency must be kept low with respect to the response of the rotor.

6.2.2 Stability Derivative Measurement: Variation in Frequency

The first technique used to validate the test process is to test whether the same value of X_u will be measured over a range of forcing frequencies and amplitudes. The simple co-axial rotor system described in section 4.7.1 was tested at frequencies between .4 and 1.6 Hz, with an oscillation amplitude of 3.5 inches for all tests. The results of those tests are shown in figure 6.1.

It is clear from figure 6.1 that a consistent value for X_u was measured between .6 and 1.2 Hz. Thus, the results exhibit the expected behavior based on stability derivative theory. At forcing frequencies below .6 Hz the reaction of the rotor does

not produce a large enough aerodynamic force reaction to be sufficiently measured by the current force balance. The insufficient force reaction causes the measured stability derivative X_u to be inconsistent from test to test and to differ from the consistent value measured at higher forcing frequencies. This result is qualitatively supported by visual observations of the rotor response. At low forcing frequencies there was little or no flapping response visible to the naked eye.

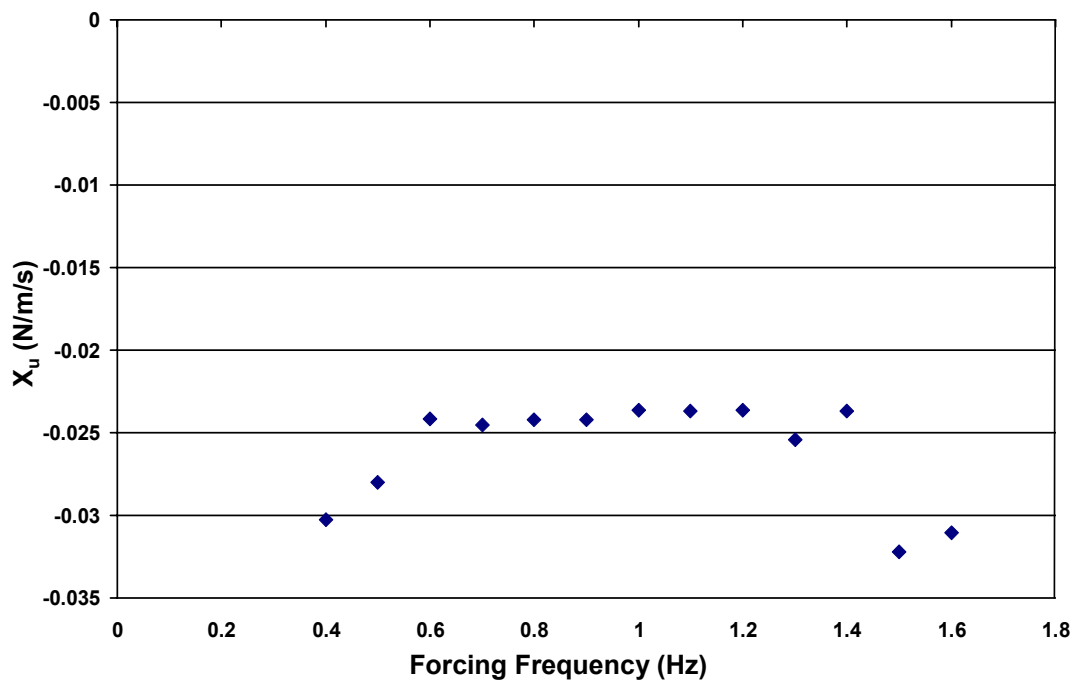


Figure 6.1 X_u vs. Forcing Frequency

At forcing frequencies above 1.2 Hz the stability derivative X_u again varies from its consistent value. This change is due to forcing frequencies which are too high with respect to the response time of the rotor system. The theory which used to determine the stability derivative considers only the force response which is in phase with the

velocity perturbation. For tests with forcing frequencies over 1.2 Hz the perturbation is either too fast for the rotor to respond at all, or there is a significant phase delay in the rotor response. From the perspective of stability derivative analysis the forcing frequency is simply too high to allow for proper determination of the stability derivative. Analysis of phase delay in the rotor response will be considered in more detail when using Bode plot representation of the data later in this section.

6.2.3 Stability Derivative Measurement: Variation in Amplitude

A similar set of measurements to those described above was taken for the measurement of X_u with forced oscillations of varying amplitudes. X_u was measured for forced oscillation amplitudes between 1.5 and 3.5 inches at a forcing frequency of .8 Hz. The results of those tests are depicted in figure 6.2.

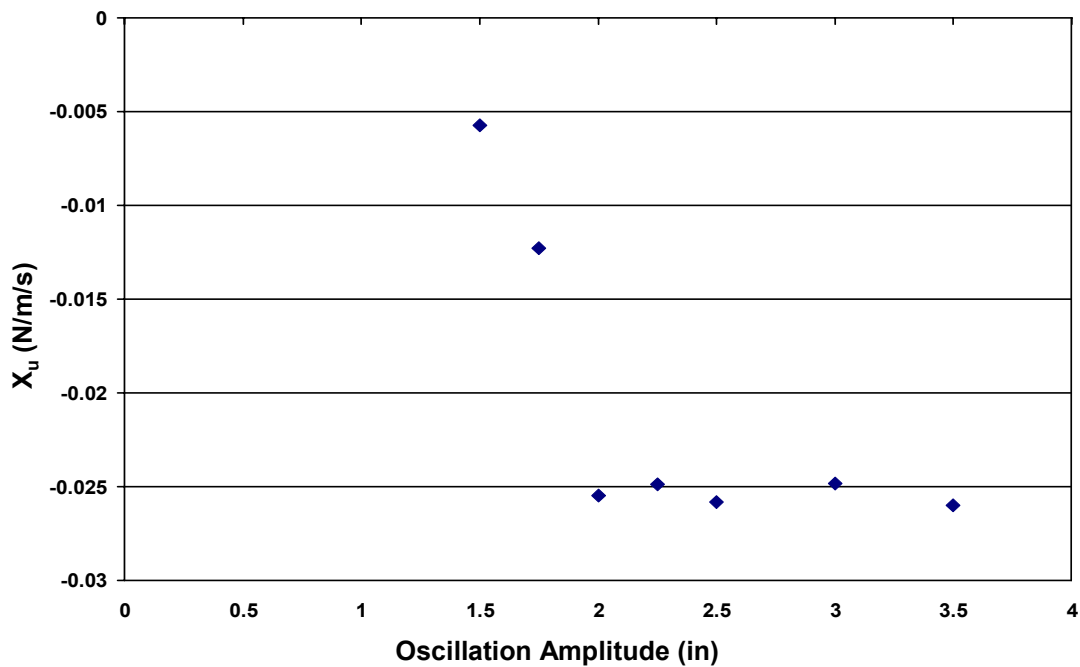


Figure 6.2 X_u vs. Oscillation Amplitude

As expected, the value of X_u measured is consistent over a range of forced oscillation amplitudes. At forced oscillation amplitudes below 2 inches however, the measured value of X_u varies from the consistent value measured at higher forcing frequencies. When the amplitude of the forced oscillation is below 2 inches the response of the rotor is once again too small to be accurately measured using the current force balance. Similar to the case of small forcing frequencies, this result was also supported by qualitative visual observations. When the amplitude of forced oscillation was below 2 inches little or no flapping response was visible to the naked eye.

6.2.4 Stability Derivative Results: Co-Axial Rotor System

The previous tests determined the value of X_u for the generic co-axial rotor system to be $-.02372$ N/m/s. Because the rotor system consists of two freely teetering rotors, the rotors can not induce a pitching moment to the rotor shaft. The pitching moment reaction that this rotor system would impart on a vehicle is therefore determined solely by the fact that the pitching moment is taken about the center of gravity of the vehicle, and the aerodynamic reaction of the rotors acts through a point offset from the vehicle's center of gravity. While the force balance used for the test above is capable of simultaneously measuring force along the X-body axis of the rotor system and pitching moment, only the X-force reaction of the co-axial rotor system was considered for the reasons detailed above. A rotor system with a rigid hub was

studied during the analysis of Bode plot representation of the data, and measurement of pitching moment is discussed in more detail at that time.

6.2.5 Qualitative Validation: Change in Rotor Collective

A way to further investigate the ability of the test apparatus to measure the stability derivatives of a vehicle is to vary the characteristics of the vehicle and observe the effects this change in vehicle parameters has on the measured stability derivatives. From this type of experiment it can be verified if the change in the measured stability derivatives matches the change predicted by a qualitative analysis of the change in vehicle properties. To perform this comparison the stability derivative X_u of a single teetering rotor was measured over a range of different collective pitch settings. This procedure was performed while holding the rotor RPM at a constant value to simulate a change in the thrust needed to hover, while maintaining the same inertia properties of the rotor. A plot of X_u vs. collective pitch angle is shown in figure 6.3. For this test the forced oscillation frequency was 1 Hz, and the oscillation amplitude was 3.5 inches.

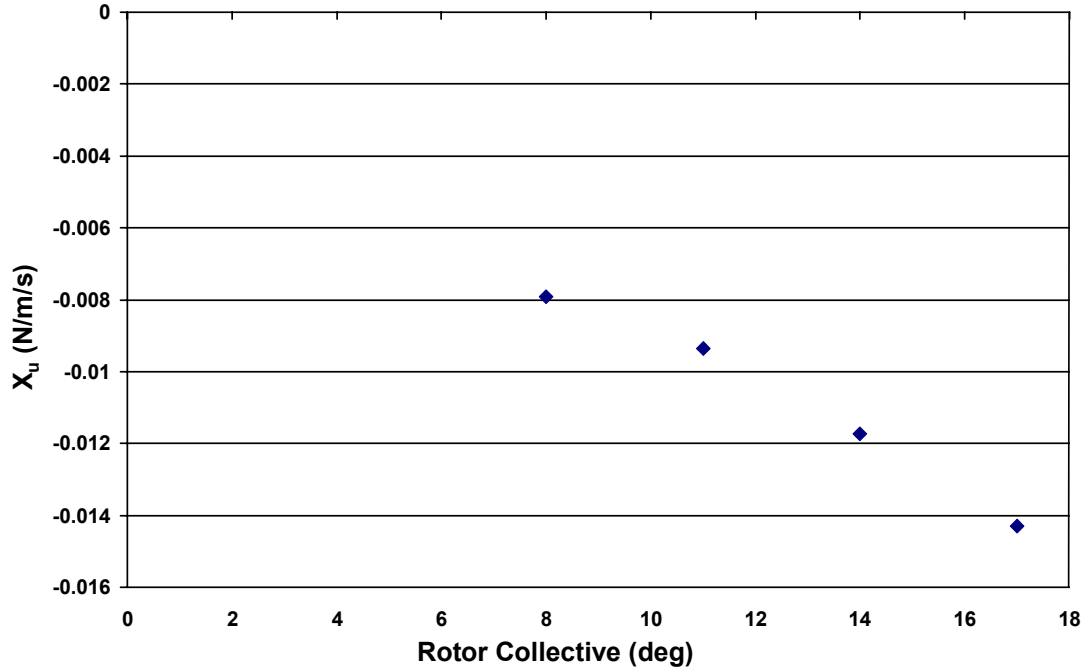


Figure 6.3 X_u vs. Collective Pitch Angle

It is apparent from the figure that as the collective pitch angle of the rotor increases, the stability derivative X_u increases in magnitude. This trend can now be compared to a simple analytical prediction of the rotor response to verify that the increase in X_u is indeed the expected trend. Prouty [7] provides a simple equation to predict the longitudinal tilt of the rotor disc for a change in forward speed.

$$\frac{\partial a_{1s}}{\partial \mu} = \frac{8}{3} \theta_0 - 2\lambda \quad (6.2)$$

In equation 6.2, θ_0 is the collective pitch setting of the rotor blades and μ is the advance ratio of the rotor. This equation assumes that the inflow through the rotor disc λ is uniform.

The velocity perturbation imparted by the forced oscillation motion causes a sinusoidal variation in the advance ratio. The amplitude of this variation in μ is determined by the amplitude of the velocity perturbation.

$$\mu = \frac{A\omega}{\Omega R} \quad (6.3)$$

By utilizing one additional assumption it is possible predict the horizontal force caused by the tilt of the rotor plane in response to the forced oscillation motion. For this simple analysis it is assumed that the thrust vector produced by the rotor is perpendicular to the rotor plane. Utilizing the measured magnitude of this thrust vector, T , and applying the assumption described above, equation 6.2 can be rearranged to provide an estimate of the force in the X-direction caused by the forced oscillation motion.

$$F_x = T \sin\left(\frac{A\omega}{\Omega R}\left(\frac{8}{3}\theta_0 - 2\lambda\right)\right) \quad (6.4)$$

Dividing equation 6.4 by the amplitude of the forced velocity perturbation produces an expression for the stability derivative X_u .

$$X_u = \frac{T \sin\left(\frac{A\omega}{\Omega R}\left(\frac{8}{3}\theta_0 - 2\lambda\right)\right)}{A\omega} \quad (6.5)$$

Clearly equation 6.5 is an overly simplified approach to approximating the stability derivative X_u . This equation is not useful as a means of producing a quantitatively accurate value. This equation is however a meaningful way to predict the expected trend for X_u as the collective pitch of the rotor is changed. It should also be noted that the results of equation 6.5 are similar to those predicted by the more comprehensive blade flapping model developed in section 6.5. This similarity supports the

conclusion that equation 6.3 is sufficient for a qualitative analysis. The values for X_u as predicted by equation 6.5, for the rotor conditions utilized during testing, are compared to the measured results in figure 6.4.

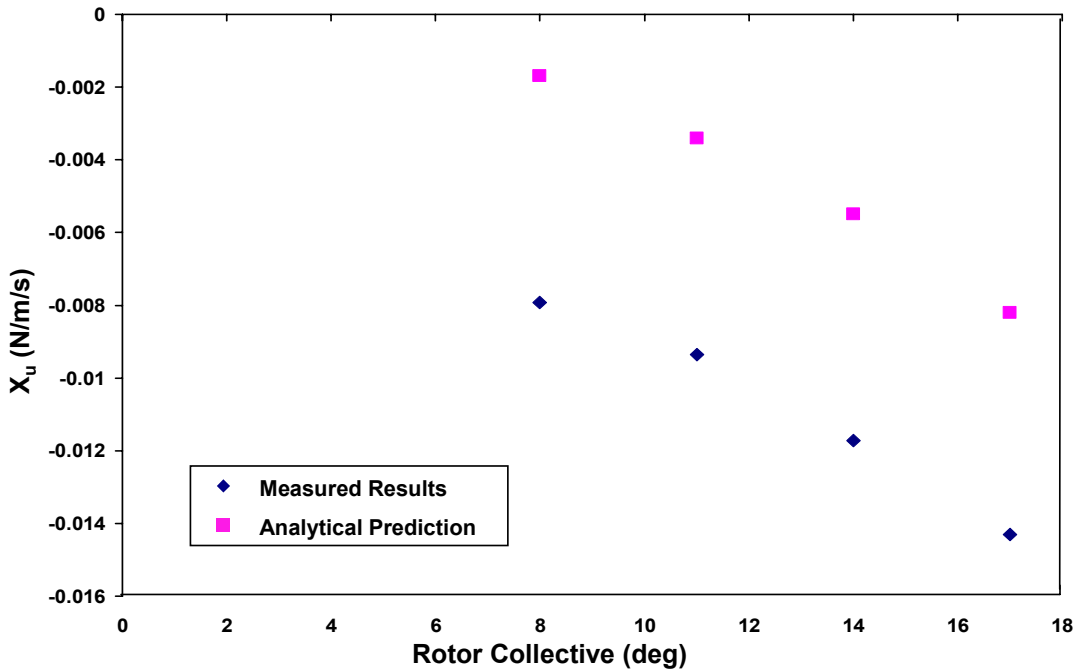


Figure 6.4 Change in Rotor Collective: Qualitative Comparison

From figure 6.4 it is clear that although the results do not match quantitatively the measured results do follow the trend predicted by the analysis. This simple analysis of the rotor response confirms that results from the forced oscillation test process are qualitatively valid.

6.3 Analysis of Results, Bode Plot Perspective

The remainder of the analysis focuses on representation of the X-force and pitching moment response of a single main rotor in Bode plot form. The objective of this analysis is to determine if Bode plot representation is a more meaningful way of

representing the rotor response to perturbations. Because the theoretical background of Bode plot representation considers the portions of the response of the rotor which are not necessarily in phase with the perturbation it is a more thorough analysis than studying only the in phase response, as is done for stability derivatives. If there is little or no phase delay present in the rotor response then Bode plot representation may be unnecessary, but for some of the rotors tested this was not the case.

6.3.1 Construction of Bode Plots

Bode plots of the rotor response were constructed by testing the rotor systems over a range of forced oscillation frequencies. Each unique test frequency results in a point on the gain and phase Bode plots corresponding to that frequency. For low frequency tests the rotors were tested at the maximum forced oscillation amplitude of 3.5 in. It should be noted that for the higher frequency tests smaller oscillation amplitudes were used in an effort to reduce the inertia loads imparted by the oscillation to within the measurable range of the force balance. Similar to the measurement of stability derivatives the amplitude of forced oscillation is not relevant to the measured points on the Bode plot of the rotor response as long as the amplitude is within the range where the force response is linear. The lower bound on this range is the condition that the perturbation in forward velocity must be large enough to induce a measurable rotor response. The upper bound on the range is such that the perturbation in velocity is low enough that the corresponding inertia loads are within the measurable range of the test setup. If the above assumption is indeed valid, the gain response of the 11 inch diameter teetering rotor should not change if the oscillation amplitude is changed. In order to check that the response is indeed consistent, the 11 inch

diameter teetering rotor was tested over a range of amplitudes at a forcing frequency of 1.8 Hz. The results of this test are depicted in figure 6.5.

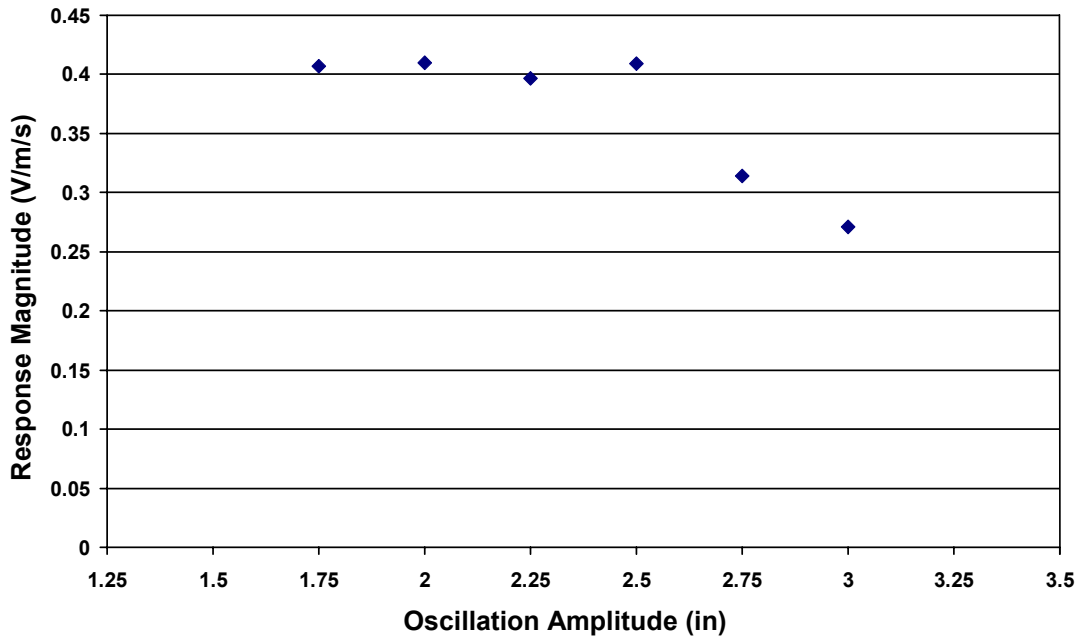


Figure 6.5 Change in Force Response for a Variation in Oscillation Amplitude

It is clear from figure 6.5 that for oscillation amplitudes between 1.75 and 2.5 inches the response of the rotor is consistent. At oscillation amplitudes above 2.5 inches the excessive inertia loads corrupt the data such that the measured response is no longer consistent. Similar results were observed for changes in amplitude at other forcing frequencies. These observations support the assumption that using smaller oscillation amplitudes at high forcing frequencies does not affect the integrity of the results. The oscillation amplitude used for each range of forcing frequency is listed in table 6.1. It was found from observation of the resulting test data that these combinations of forcing amplitude and frequency are within the range of linear response.

Forcing Frequency (Hz)	Oscillation Amplitude (in)
.4 – 1.2	3.5
1.3 – 1.6	2.5
1.7 – 2	2
2.1 – 2.2	1.5
2.3 – 2.5	1

Table 6.1 Selection of Oscillation Amplitude

6.3.2 Teetering Rotor System

The first rotor tested was the freely teetering 11 inch diameter rotor described previously in the test setup section. A Bode plot of the X-force response of this rotor to perturbations in velocity along the X-body axis of the rotor system is shown in figure 6.6. It should be noted that because this is a teetering rotor there is virtually no moment applied to the rotor shaft by the flapping response of the rotor. For this reason only the X-force response was considered.

From figure 6.6 it is clear that the measured gain of the rotor system is not consistent as the forcing frequency changes. Rather, it appears that the X-force response increases as frequency increases. For this reason we identify that a constant coefficient stability derivative is most likely not sufficient to represent the response of this rotor. The Bode plot representation is still a useful representation however as it depicts the X-force response of as a function of frequency. An additional observation can be made from the phase response of the rotor. It is clear from the Bode plot that

there is significant phase delay in the system. This phase delay increases as the forcing frequency of the system increases. For this rotor system the assumption of an instantaneous rotor response is most likely not sufficient. For this reason the Bode plot representation is more useful than simply defining the response with a stability derivative approximation.

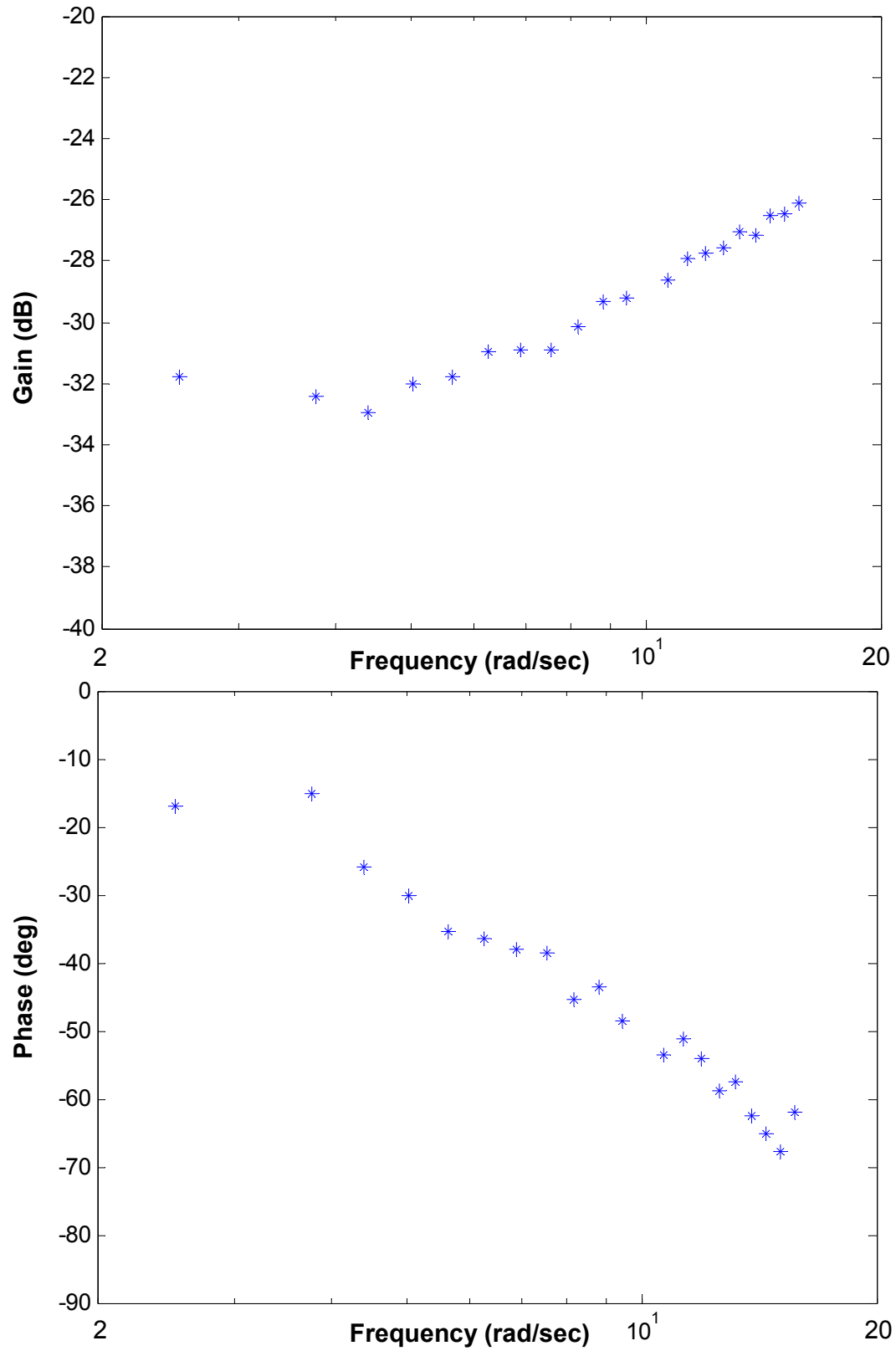


Figure 6.6 Bode Plot of Teetering Rotor X-Force Response

An additional consideration of the test results is the correlation between the measured aerodynamic response and the forced velocity perturbation. As discussed in section 5.6.3, the correlation between the input perturbation and the output aerodynamic reaction is a way to quantify the degree of linearity between the two signals. In practice, the correlation measurement is a good way of assessing the strength of the reaction signal with respect to the noise present in the measurements. A plot of correlation versus forcing frequency for the 11 inch teetering rotor is depicted in figure 6.7. It should be noted that for these measurements the reaction signal has been low-pass filtered at 20 Hz.

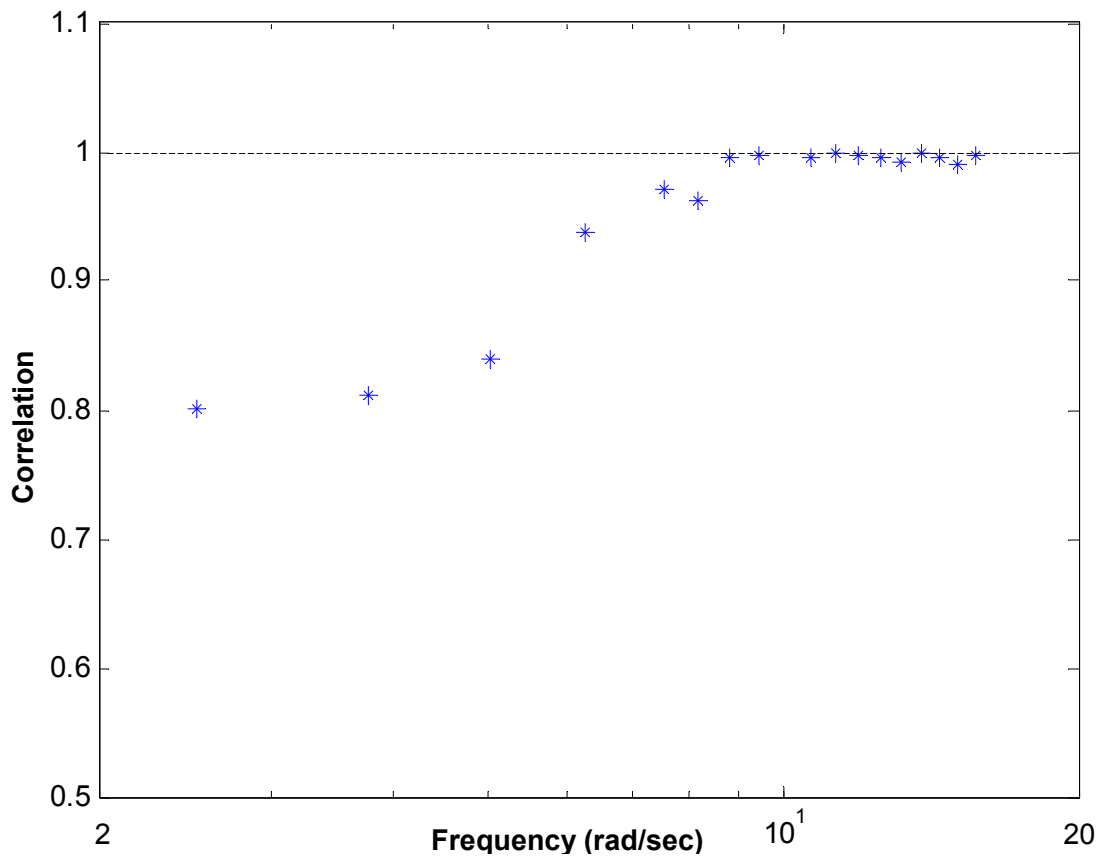


Figure 6.7 Correlation vs. Frequency for 11" Teetering Rotor

From figure 6.7 it is clear that at low frequencies the correlation between the perturbation and the response is significantly less than one. This indicates the presence of considerable noise in the measurement of the aerodynamic force reaction. This is however a reasonable result. At low forcing frequencies the magnitude of the aerodynamic reaction force is relatively small, thus it is possible for noise in the system to be of large enough magnitude as to corrupt the signal. At higher forcing frequencies the aerodynamic reaction is larger and more clearly defined. Thus, the signal is less easily corrupted by small vibrations and other noise present during testing. The reduction in the measured correlation at low forcing frequencies is clear from observations of the response signal at low frequencies. Figure 6.8 depicts the aerodynamic response signal for the 11 inch teetering rotor for a forcing frequency of .6 Hz. A similar plot of the response of the 11 inch teetering rotor at a forcing frequency of 1.8 Hz is depicted in figure 6.9.

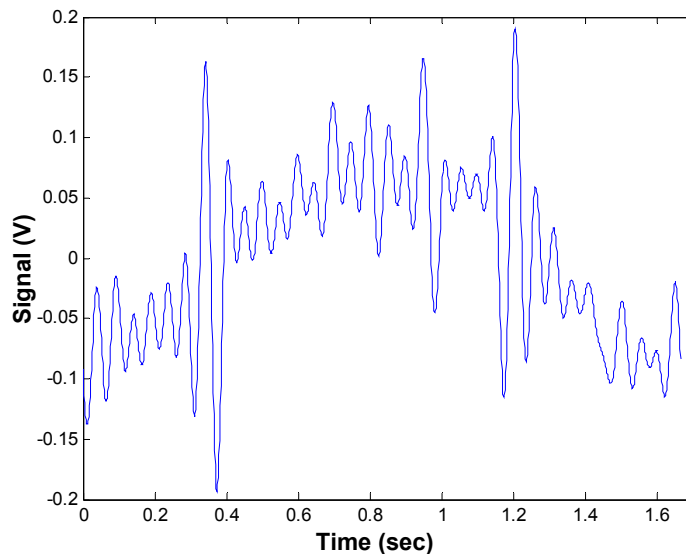


Figure 6.8 Response Signal for 11" Teetering Rotor at .6 Hz

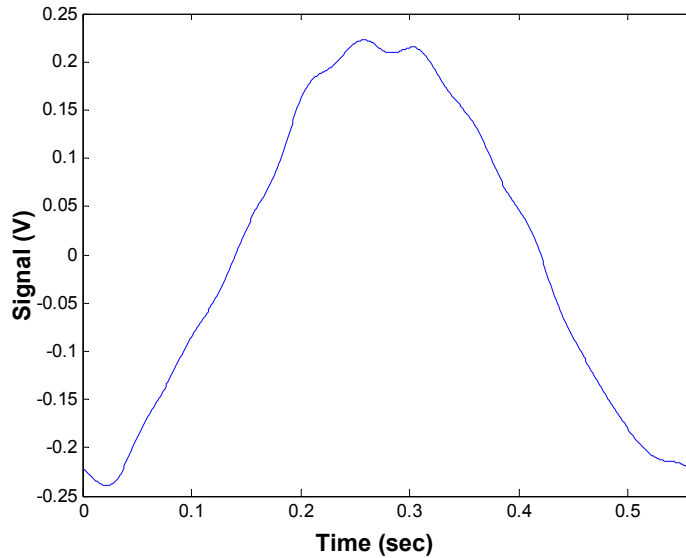


Figure 6.9 Response Signal for 11" Teetering Rotor at 1.8 Hz

Comparison of figures 6.8 and 6.9 reveals why the correlation measurement for low forcing frequencies is significantly less than one. The considerable noise in the response signal at a forcing frequency of .6 Hz reduces the correlation between the velocity perturbation and the reaction measurement to .8116. From figure 6.9 it is clear that the response signal has much less distortion due to noise in the signal. This corresponds to a higher correlation between the perturbation and the reaction signal, a value of .9987. Correlation analysis suggests that for improved measurement of the rotor response at low frequencies it may be necessary to increase the magnitude of the rotor response. This could be obtained utilizing larger oscillation amplitudes at low forcing frequencies. Because the current test stand is limited to oscillations of 3.5 inches in magnitude, these higher amplitude tests are outside the current testing capabilities. The result is however still useful as a suggested improvement to the test

setup if the response of rotary wing MAVs at low frequencies is of considerable interest.

Analysis of the test results for the 11 inch diameter teetering rotor from a Bode plot perspective provides several useful observations. The information that can be concluded from this analysis is as follows:

- The gain portion of the Bode plots indicates that the response of the rotor is not consistent with changing frequency.
- There is considerable phase delay in the rotor response at high forcing frequencies.
- Because of an inconsistent response and considerable phase delay the approximation of the rotor response by a stability derivative may not be appropriate
- The correlation between the input velocity perturbation and the output rotor response is considerably less than one at low forcing frequencies.

6.3.3 Rigid Hub Rotor System

The next rotor tested for Bode plot analysis was the 11 inch diameter rotor with a rigid hub. Because the rotor is no longer a teetering configuration a moment can be applied to the rotor shaft by the response of the rotor to perturbations. Because a pitching moment response to a perturbation in forward velocity is expected, Bode plots of both the pitching moment response and the X-force response were constructed. These plots are shown in figures 6.10 and 6.11.

From the gain portion of plots 6.10 and 6.11 it is clear that the pitching moment response of the rotor system is more consistent than the response of the

teetering rotor over the range of forcing frequencies tested. The X-force response is not as consistent as the pitching moment response, but it should be noted that the magnitude of this response is quite small. For this reason, the gain response of the rigid rotor could be approximated more closely than the corresponding response of the teetering rotor by a constant coefficient stability derivative. Observation of the phase plots reveals that the phase delay present in the response of this rigid hub rotor system is much smaller than that of the equivalent teetering rotor. Because the orientation of the tip path plane of the rotor does not need time to establish itself, the rigid rotor responds more quickly to perturbations. The rigid rotor has a more consistent gain response and less prominent phase delay than the equivalent teetering rotor. For this reason the response of the rigid hub rotor system could be approximated more accurately by a stability derivative than the teetering rotor. Clearly, the Bode plot representation lends additional insight into the response of the rigid rotor, but a stability derivative representation might still be an acceptable simplification for certain applications.

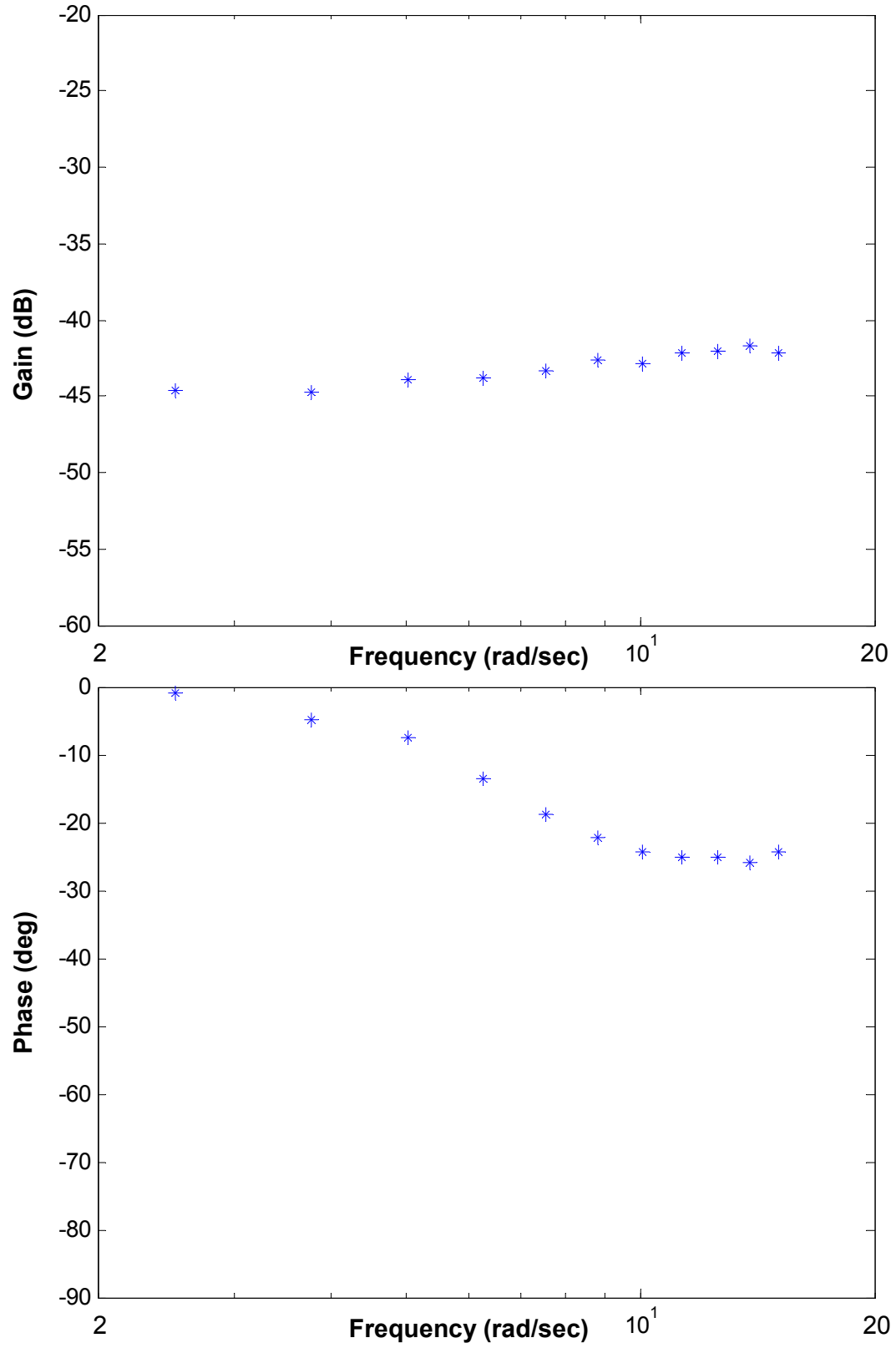


Figure 6.10 Bode Plot of Rigid Rotor Pitching Moment Response

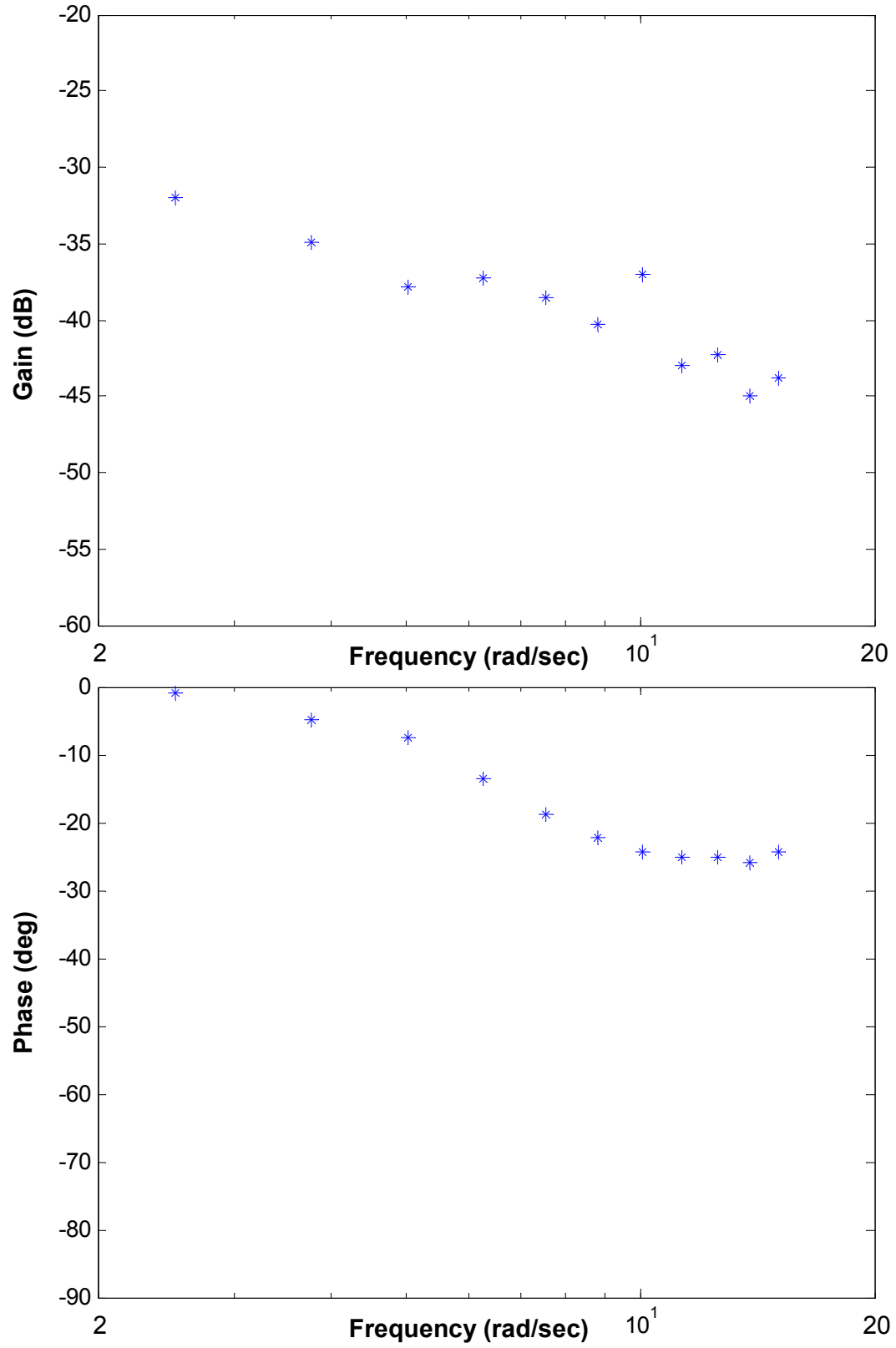


Figure 6.11 Bode Plot of Rigid Rotor X-Force Response

Similar to the analysis performed for the 11 inch diameter teetering rotor, the correlation between the response of the rigid rotor and the forced velocity perturbation was also considered. These correlation measurements are plotted versus forcing frequency in figure 6.12.

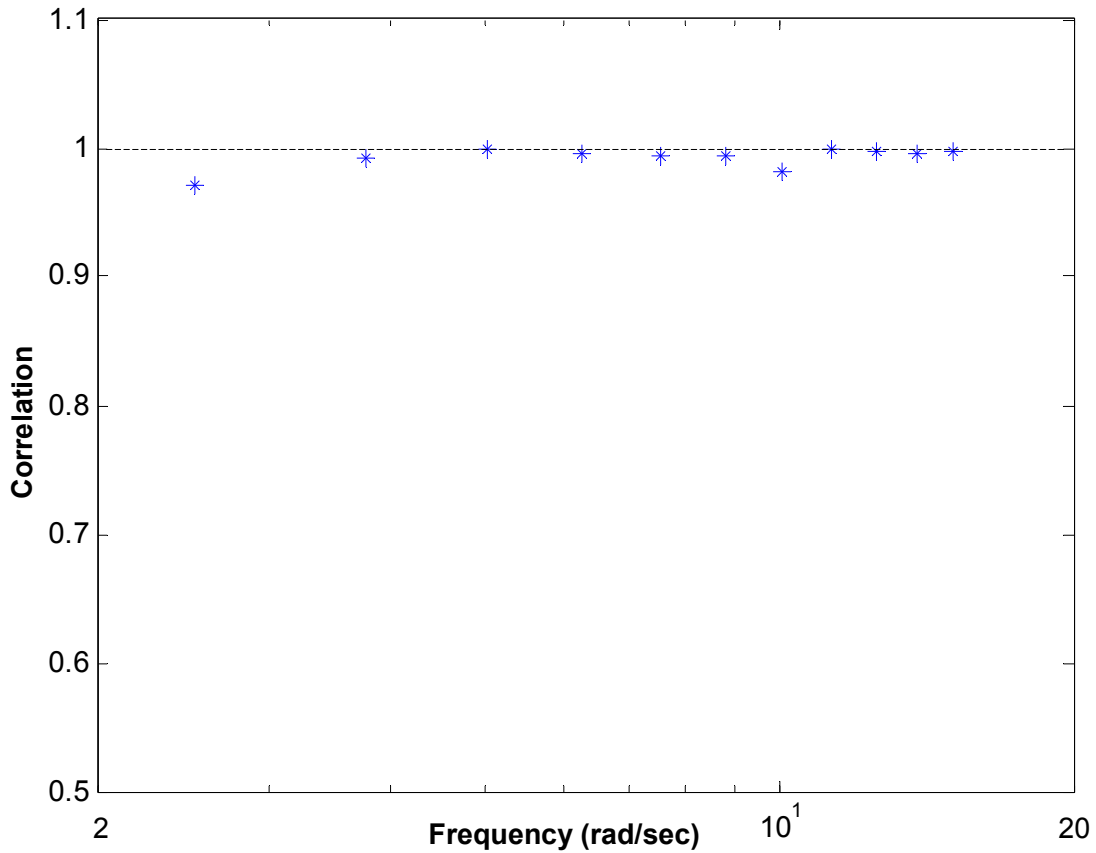


Figure 6.12 Correlation vs. Forcing Frequency for 11" Rigid Rotor

From figure 6.12 it is clear that the correlation between the aerodynamic response and the velocity perturbation is nearly one over the entire range of forcing frequencies. This is significantly different than the result observed for the teetering rotor, where the correlation was considerably less than one for low forcing frequencies.

Additional insight into this discrepancy can be gained from observation of the aerodynamic response signal for the rigid rotor. The response signal is depicted in figure 6.13 for a forcing frequency of .6 Hz.

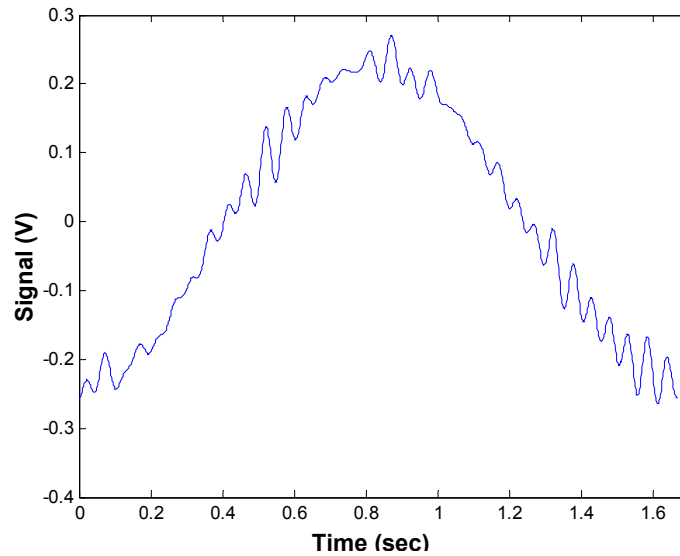


Figure 6.13 Response Signal for 11" Rigid Rotor at .6 Hz.

Comparison of figure 6.13 to the corresponding figure for the teetering rotor, figure 6.8, reveals the reasoning for the difference in correlation measurements between the two rotors. For the rigid rotor the magnitude of the noise when compared to the signal strength is significantly less than for the teetering rotor. The primary reason for this discrepancy is that the magnitude of the rotor response is larger; reducing the amount the signal is corrupted by the noise. Additionally, it is possible that the rigid configuration of the rotor system is less susceptible to vibrations of the test setup.

The Bode plots and correlation analysis for the 11 inch diameter rigid rotor provide several useful observations. These conclusions are as follows:

- The pitching moment response of the rotor is fairly consistent over the range of forcing frequencies.
- The phase delay of the response is fairly small, less than 30 degrees.
- Because the gain response is consistent and the phase delay is small the response could potentially be approximated by a stability derivative.
- The correlation between the aerodynamic response and the velocity perturbation is nearly one over the entire range of forcing frequencies.

6.4 Comparison of Data Representation Techniques

The various tests described in the previous sections provide a good basis of comparison between the techniques of representing the response of the rotor as a stability derivative or in Bode plot form. It is clear from the analysis of Bode plot representation that the response of some rotors which could potentially be implemented on rotary wing MAVs can not be satisfactorily described using simple stability derivatives. Because of the broader range of information depicted by Bode plots they are initially more useful as a means to represent the response of the rotor. Analysis of the Bode plots can also be utilized to determine if a simplified stability derivative approximation could be considered for the rotor system in question. If it is indeed decided that a stability derivative approximation is sufficient, it is trivial to convert the gain plot of the rotor response to a constant stability derivative. For these reasons, it is recommended that for initial tests of a vehicle or rotor system the response should be analyzed in Bode plot form.

6.5 Analytical Validation of Test Results

The current test setup exhibits all of the expected results from a qualitative point of view. Simple analysis of several example rotor systems suggests that the test process is a valid way of measuring the stability parameters of MAV scale rotor systems and potentially entire vehicles. The analysis performed thus far however lends little insight into the quantitative accuracy of the test results. Development of an accurate quantitative prediction of the rotor response is a challenging task. Inherent difficulties in analyzing the rotor response with traditional techniques were the motivation for the current research in the first place. Ideally, results from forced oscillation testing of a flight worthy MAV would be compared to system identification results from flight test data. Because system identification flight testing is not yet feasible for any of the available MAVs another comparison must be used. The following sections discuss a simple analytical approximation of the blade flapping response of the 11 inch diameter teetering rotor. This approximation is then compared to results from forced oscillation testing.

6.5.1 Numerical Analysis of Blade Flapping Motion

The most feasible method for analytically predicting the response of a rotor system to perturbations is by analysis of the equations of motion for rotor blade flapping. A model of the flapping response to changes in advance ratio was constructed from the differential equations for blade flapping motion. These blade flapping equations are discussed in more detail by Leishman [43]. Additional analysis of simple blade flapping equations is covered by Chen [44], [45]. The most general equation for the flapping motion of a rotor blade with uniform mass distribution is given as

$$I_b \ddot{\beta} + I_b \Omega^2 \beta = \int_0^R L y dy \quad (6.6)$$

Where β is the flapping angle of the blade, I_b is the moment of inertia of the blade about the flapping hinge, and L is the incremental value of lift on the blade at radial location y . L is given as force per unit length as shown below.

$$L = \frac{1}{2} \rho U_T^2 c C_{l\alpha} \left(\theta - \frac{U_p}{U_T} \right) \quad (6.7)$$

U_t and U_p are the tangential and perpendicular velocity components at the blade section as given by

$$U_T = \Omega R \left(\frac{y}{R} + \mu \sin \psi \right) \quad (6.8)$$

$$U_p = \Omega R \left(\lambda + \frac{y \dot{\beta}}{\Omega R} + \mu \beta \cos \psi \right) \quad (6.9)$$

Inserting equations 6.7, 6.8 and 6.9 into equation 6.6 yields differential equations for blade flapping motion. These differential equations can be numerically solved using MATLAB to give a time history of the blade flapping response to a change in μ . The variation in μ as a function of time is sinusoidal in nature as defined by the forced oscillation motion. In order to model the flapping motion of a teetering MAV scale rotor several modifications to the standard flapping equation are needed. First, both blades of the teetering rotor are considered simultaneously. The flapping angle of blade two is the negative of the flapping angle of blade one, as constrained by the teetering hub. Also, the lift generated by each blade is considered separately, as L_1 and L_2 are the values of incremental lift on blades one and two respectively. These modifications result in the new blade flapping equation below.

$$2I_{\beta}(\ddot{\beta} + \Omega^2\beta) = \int_0^R L_1 y dy - \int_0^R L_2 y dy \quad (6.10)$$

The second potential modification is a variation in the lift curve slope $C_{l\alpha}$ with respect to radial location along the blade. The intent of this change is to model the effect of change in the lifting properties of the blade due to Reynolds number variation over the blade span. It should be noted that after studying several variations in the radial distribution of $C_{l\alpha}$ it was determined that the shape of the distribution had little effect on the flapping response. For that reason, the remainder of the analysis considers a constant value for $C_{l\alpha}$ along the span of the blade.

6.5.2 Comparison of Numerical Analysis to Experimental Data

The differential equations for blade flapping described above were solved using MATLAB for a representative forced oscillation test. A time history result for the blade flapping angle β , of a rotor with the same characteristics as the 11 inch diameter teetering rotor is shown in figure 6.14. For this simulation the velocity perturbation is representative of a forced oscillation test with an amplitude of 3.5 inches at a forcing frequency of 1 Hz.

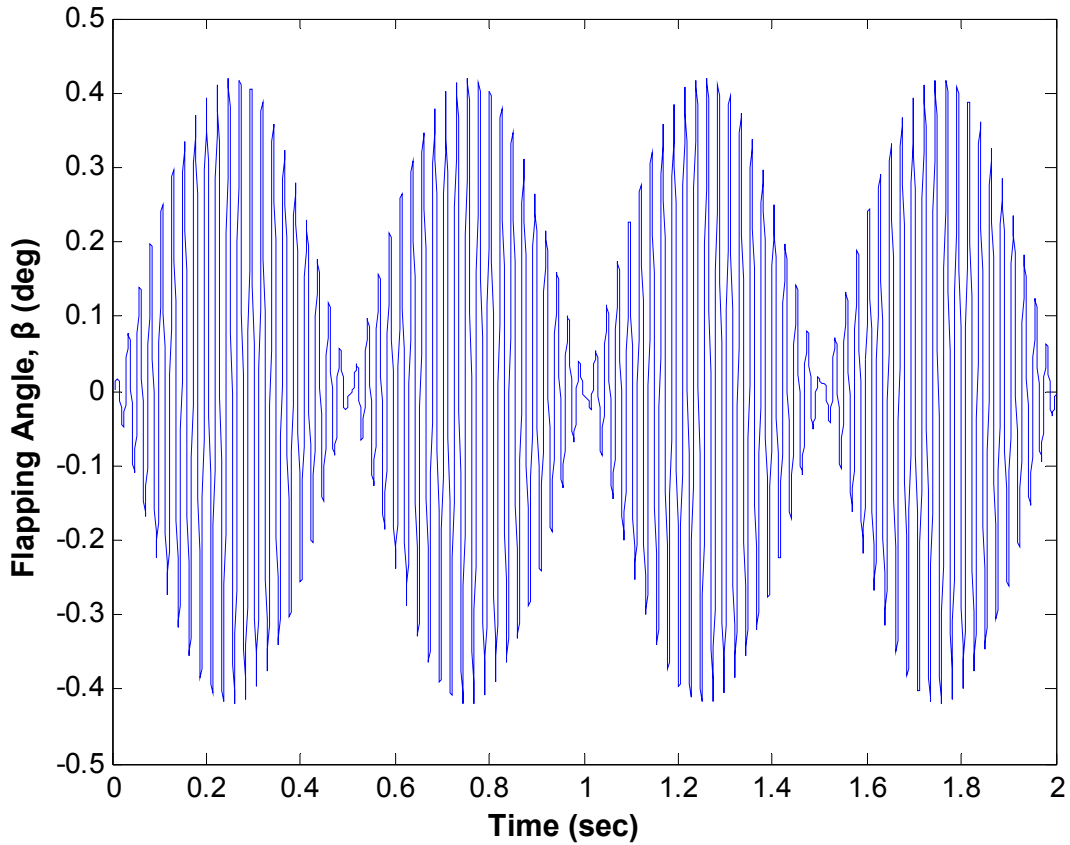


Figure 6.14 Flapping Angle vs. Time

From figure 6.14 it can be determined that the amplitude of the longitudinal flapping angle is 0.4202 deg. Similar simulations were performed over a range of test conditions representative of the forced oscillation tests performed on the 11 inch diameter teetering rotor. The results of these simulations are listed in table 6.2.

Forcing Frequency (Hz)	Flapping Amplitude (deg)	$\beta/A\omega$ (deg/(m/s))
1	0.4202	0.7522
1.2	0.5042	0.7521
1.4	0.5879	0.7518
1.6	0.6720	0.7519
1.8	0.7561	0.7520
2	0.8403	0.7521

Table 6.2 Flapping Response from Analytical Calculations

From the table it is clear that the numerical analysis predicts a constant value for the longitudinal flapping per unit of velocity perturbation about hover. By making the simple assumptions that the thrust vector of the rotor is perpendicular to the tip path plane of the rotor and the thrust produced by the rotor is constant, the predicted value for the longitudinal flapping angle can be used to estimate the expected force response of the rotor. The predicted force response can then in turn be converted to Bode plot form as the expected gain of X-force per unit of perturbation in forward velocity. This result is shown compared to the measured X-force response for the 11 inch diameter teetering rotor system in figure 6.15.

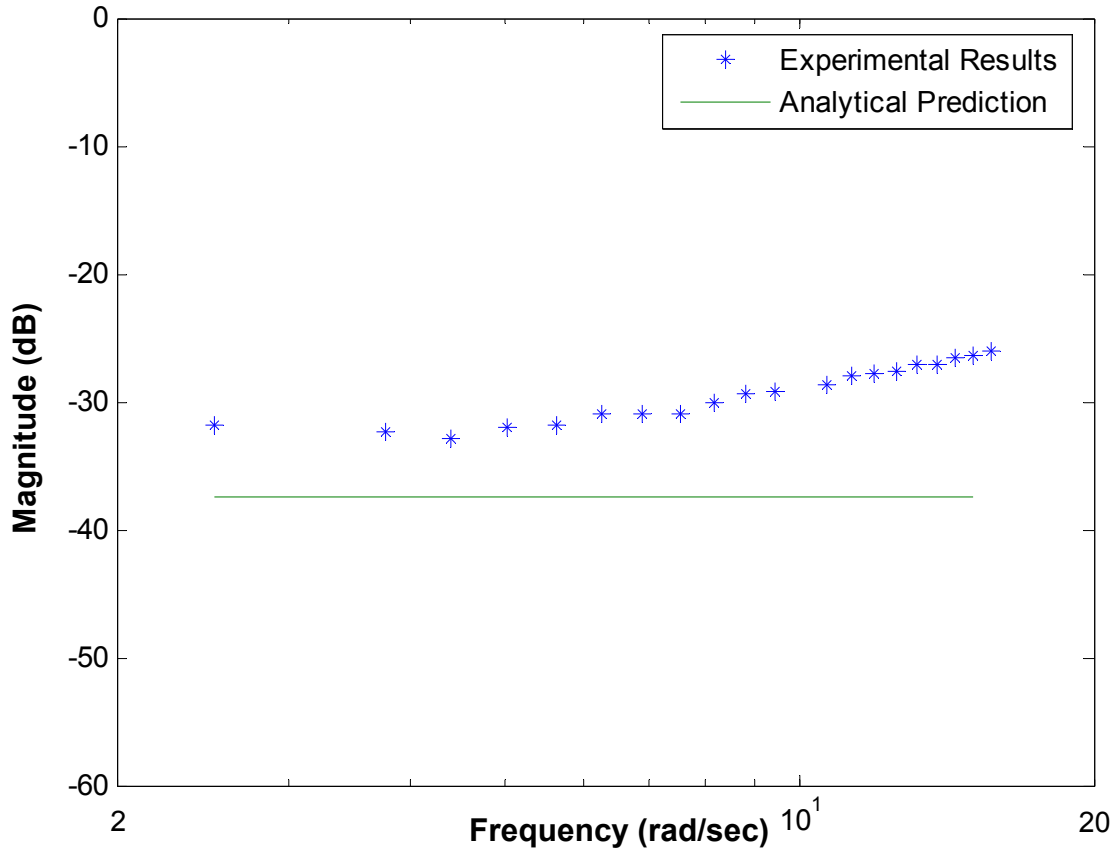


Figure 6.15 Comparison of Analytical and Experimental Results

From figure 6.15 it is clear that numerical analysis of the blade flapping equations of motion under predicts the flapping response. While the results from numerical analysis do not match well with those determined experimentally, the results are well within the same order of magnitude. This result suggests that the test technique is returning reasonable values for the force response of the rotor. Once sufficient flight test data becomes available, a more thorough qualitative analysis will become possible.

6.6 Application of Results

In sections 6.2 and 6.3 forced oscillation testing has been used to determine a few of the dynamic characteristics of example rotor systems for a hovering flight condition. In a scenario where an actual vehicle was being studied for stability and control analysis, the results would now be applied to a vehicle model. This is fundamentally the same process that is used in system identification flight testing. This technique involves developing a parameterized model of the vehicle from first-principles. The parameters of this model are then identified by tuning the parameters of the model such that the model matches the response measured during flight testing. This process is described in detail by Mettler [22]. The results from forced oscillation testing are essentially used in the same way. The measured values for M_u and X_u would be applied to a model of the vehicle containing those parameters. The development of such a model is outside the scope of the current research, but the construction and use of similar models is well documented.

The dynamic characteristics identified from forced oscillation testing could also be used in a more basic analysis of vehicle motion. One such case is analysis of the longitudinal dynamics of the vehicle about hover. Simplified, linearized equations of motion for the “fixed-stick” longitudinal dynamics of a full size helicopter are given below. These equations may not necessarily capture the dynamics of a MAV, but they are most likely sufficient for an initial analysis.

$$\begin{aligned} \dot{u} - X_u u - X_q q - g\theta &= 0 \\ \dot{q} - M_u u - M_q q &= 0 \\ \dot{\theta} &= q \end{aligned} \tag{6.11}$$

From Equation 6.11 it is clear where the measured results from the forced oscillation testing, M_u and X_u , are applied. These results are not necessarily useful however, without similar results for the parameters M_q and X_q . As discussed previously, the ability to only determine a few vehicle parameters at once is a shortcoming of the forced oscillation technique. If a forced oscillation test stand capable of determining the values of M_q and X_q were developed, a more comprehensive analysis of the longitudinal dynamics of a rotary wing MAV would be possible.

6.7 Additional Observations

Qualitative observations of the test process lend some additional insight into the response of the tested rotor systems to perturbations in forward velocity. For the teetering rotor systems, both co-axial and single rotor, the longitudinal flapping response of the rotor is clearly visible to the naked eye. This observation is quite useful in confirming that the tip path plane of the rotor system does indeed tilt back in response to the perturbation in forward velocity. Observation of the flapping response of the rotor also supports the result of negligible change in the orientation of the tip path plane for forced oscillations where the combination of forcing frequency and amplitude is too small.

An even more interesting visual observation is the out of plane flapping response of the rotor. It is clear from watching the response of the rotor during testing that a perturbation in forward velocity does not induce a purely longitudinal flapping response. Because of the teetering nature of the rotors in question and the

absence of any coning angle, the response should be purely longitudinal for uniform inflow. As discussed in section 4.9 however, some lateral flapping is expected due to non-uniform inflow effects. This effect is described in more detail by Padfield [38]. For perturbations about a hover condition the lateral flapping response is potentially of the same order of magnitude as the longitudinal response. This is indeed confirmed from observations of the rotor during testing. Although it is outside the scope of the current research, this side force response could be quantified by using a variation of the current test setup. By changing the orientation of the force balance by 90 degrees, the side force and rolling moment response of the rotor systems could be measured.

One final aspect of the test stand which must be considered is the interference of the stand itself with the wake of the rotor system or vehicle in question. It is possible that portions of the test stand could cause the rotor to be in partial ground effect at different times during the forced oscillation tests. For traditional rotor testing, such as thrust and torque a measurement of a hovering rotor, the rotor is inverted such that the flow through the rotor is in an upward direction. This change in rotor orientation effectively serves to remove the possibility of the rotor being in a ground effect situation during testing. The forced oscillation test stand used in this research was not originally designed to test inverted rotors. Because the ultimate goal of forced oscillation testing is to test entire vehicles, it is important that the rotor downwash passes over the fuselage of the vehicle just as it would in an actual flight condition. For this reason inverting the rotor is not reasonable. It is still important however to ensure that the test stand is not unnecessarily interfering with the wake of

the rotor. Because only rotor systems and not entire vehicles were tested for this initial research, it is possible to invert the rotors. In order to determine if the rotor wake was being significantly affected by the test stand in the tests described above the 11 inch diameter teetering rotor was tested in an inverted orientation. The results of this test for several different frequencies are compared to the initial test results in figure 6.16.

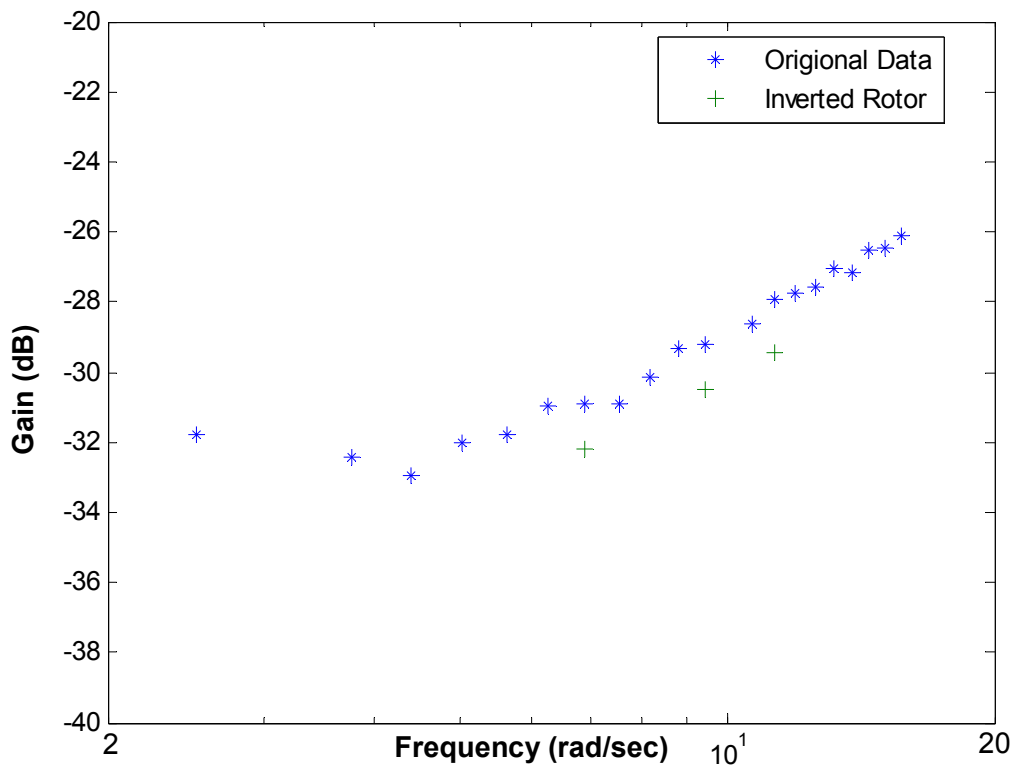


Figure 6.16 Inverted Rotor Comparison

From figure 6.16 it is clear that the gain response for the inverted rotor is slightly less than that originally measured with the rotor in a standard orientation for all three forcing frequencies tested. From this observation it can be concluded that there is

potentially some unwanted interaction between the rotor wake and the test stand. It appears however that the interaction is small and does not affect the trend of the measured data. It is still advisable however to test the rotor systems in an inverted orientation if possible. If it is not possible to invert the rotor, additional steps could be necessary to increase the distance between the rotor and the main structure of the test stand. By increasing the distance between the base of the test stand and the rotor it would be possible to eliminate the interaction of the rotor wake and the stand itself.

6.8 Conclusions

In conclusion, initial tests of representative small scale rotor systems have shown the ability of the forced oscillation test process to measure the stability characteristics of the rotor systems. Qualitative analysis of the test results shows that the test process is returning the expected results. Additional analysis of the different methods of representing the data shows that for some example rotor systems the representation of the rotor response by a stability derivative is not sufficiently accurate. For the initial analysis of a rotor system it is much more comprehensive to first determine the Bode plot of the response and then simplify the representation to a stability derivative if appropriate.

Comparison of the measured results to an analytical model shows that the test process is providing reasonable values from a quantitative point of view. The experimental results do not closely match the analytical prediction but this is to be expected. The analytical model does however confirm that the magnitude of the measured results is within the expected range. The absence of a more accurate

analytical model to predict the rotor response is inherently one of the motivations for the development of the forced oscillation test process.

The following chapter will provide a summarization of the research project and present some concluding remarks. Recommendations for future work on the subject are also offered.

Chapter 7: Concluding Remarks

7.1 Summary and Conclusions

This thesis has presented a testing technique for measuring the stability parameters of rotary wing MAVs. The technique uses a forced sinusoidal motion to induce a perturbation in flight conditions and measures the corresponding reaction of the vehicle.

The small scale of rotary wing MAVs make the development of an accurate dynamic model a challenging task. Many of the standard methods for measuring the stability parameters of full size rotorcraft are not currently feasible for vehicles of this scale. The potential uses for rotary wing MAVs often require autonomous control of the vehicle. Development of effective autonomous controllers will be greatly aided by accurate dynamic models of the vehicles. For that reason there is sufficient motivation to explore forced oscillation testing as an alternative way of determining MAV stability parameters experimentally.

The theoretical development of the forced oscillation technique utilizes a simple sinusoidal perturbation to vehicle flight conditions. The corresponding response to this perturbation is also assumed to be sinusoidal in nature. Because of these simplifying assumptions, the stability characteristics of the vehicle can be easily determined from a Fourier series approximation of the aerodynamic force response.

There are two different ways to present the stability characteristics, either by a constant coefficient stability derivative or by a Bode plot.

The current forced oscillation test setup utilizes a scotch yoke mechanism to impart a velocity perturbation along the X-axis of the vehicle under consideration. The corresponding X-force and pitching moment response is measured using a strain gauge force balance. This force and moment response as well as a synchronized vehicle position measurement are recorded using a digital data acquisition system. The corresponding digital data files are analyzed using MATLAB and can be reduced to meaningful stability parameters.

Several representative rotor systems were tested as a means of validating the test procedure. Initially analysis of the test results was considered from a stability derivative perspective. It was shown that the measured stability derivatives of a simple co-axial rotor system qualitatively matched the expected results. As a more thorough means of measuring the stability parameters of a MAV, Bode plots were formulated for two 11 inch diameter rotors. From these plots it was shown that for the 11 inch teetering rotor stability derivative representation of the rotor response would most likely not be sufficient. It was also shown however that the response of the rigid rotor could be approximated by a stability derivative more accurately. In order to properly describe the response of the tested rotors it was concluded that first a Bode plot should be constructed and then the simplification to a stability derivative could be made if appropriate.

In order to quantitatively validate the measured results an analytical model of the blade flapping response was developed. The comparison of this model to the

experimental measurements revealed that although the model did not closely match the measurements the two results are similar in magnitude. This finding supports the conclusion that the test process is returning reasonable values for the stability parameters of the tested rotor systems.

7.2 Recommendations for Future Work

Due to the developmental nature of the current research many lessons have been learned regarding the application of forced oscillation testing to rotary wing MAVs. In order to efficiently continue with development of this technique as a useful tool for the testing of MAVs it is important to consider these lessons as future research progresses. This section will serve to recommend future research as well as comment on other issues not covered in the previous sections of the document.

Through several iterations of development, it has become clear that the most pivotal element in the test setup is the force balance. Because of the relatively high inertial loads and comparatively small aerodynamic forces, the force balance must be designed to measure moderately large forces while remaining as sensitive as possible. Additionally, a six degree of freedom force balance would be preferable compared to the cantilevered beam currently in use. This more sophisticated force balance would allow for determination of six rotor stability parameters simultaneously while the current balance is only capable of measuring two. A primary concern for the design of an improved force balance is that it must remain relatively rigid as to not violate the assumption that the motion of the linear slide is perfectly transferred to the test vehicle. Additionally, it should be noted that a balance which separates the individual forces and moments mechanically is preferred over one which separates coupled

forces and moments. In order to separate coupled forces and moments, as is done for the current test setup, the assumption must be made that the force and moment response is synchronized. This is of course not necessarily a valid assumption. It is perfectly feasible that some of the force and moment responses could be nearly instantaneous while others exhibit considerable phase delay.

A force balance designed to measure force in the X-direction while mechanically separating other force inputs was designed and implemented for the forced oscillation test stand. This force balance consists of an aluminum frame with two vertical brass flexures. These flexures allow an S-shaped displacement when a force is applied to the balance in the X-direction, but remain comparatively stiff in response to other forces and moments. A thin beam load cell bonded to one of the flexures was used to measure the X-force. While this force balance was quite capable of separating the X-force from other applied forces and moments and was relatively sensitive it was ultimately not effective. It was found that unnecessarily high inertia loads caused by the force balance itself corrupted the measurement of the aerodynamic response forces. After several attempts to modify the force balance it was determined that the cantilevered beam was a more effective means of measuring force in the X-direction.

The forced oscillation test stand developed for initial testing and validation is designed to induce a velocity perturbation to the vehicle or rotor system along the X-body axis of the vehicle. This choice of perturbation was chosen because of the simplicity of the apparatus needed to induce a sinusoidal perturbation. The simple mechanism design along with the important rotor flapping response induced by this

type of perturbation made it a logical choice for a development study. Now that the technique has shown favorable results it is likely that there may be interest in developing additional forced oscillation test stands. It is recommended that the first consideration should be the design of a test stand capable of producing sinusoidal variation in the pitch angle of the vehicle. The pitching and rolling response of current MAV design concepts is of fundamental importance from a stability and control perspective. A forced pitching oscillation test stand would allow for experimental analysis of these characteristics. The use of stabilizer bars has proven fundamental in the design of MICOR [2]. A test stand capable of measuring the force and moment response to a pitching perturbation would allow for testing of stabilizer bars and other similar stability augmentation devices. This type of test stand would also induce a forced oscillation motion that would create much smaller inertial loads while sufficiently applying the perturbation to flight conditions. This advantage would allow a more sensitive force balance, which is a primary concern in the measurement of small reaction forces, as discussed above.

Appendix A: MATLAB Program Code, “mavplotDZ”

```
%Usage: mavplotD(<filename 1>,<filename 2>,<sample rate>,<forcing  
%frequency>,<length of test>,<number of terms retained in FFT>)  
%Takes the data from each test run (1,2) and averages it for each  
%cycle Then uses the position data to reduce the force data to  
%exactly 1 oscillation where each data point is actually the average  
%force for that position over the entire test run. Then takes the  
%two results and filters them using FFT. Returns the magnitude and  
%phase of both the tare test and the rotors-on test. Also returns  
%the filtered representation of those tests for use in the program  
%mavavD
```

```
function [mf_off,mf_on,U_off,U_on,t] =  
mavplotDZ(filenameoff,filenameon,sampPERsec,freq,legnth,terms)
```

```
datalegnth = sampPERsec*(1/freq);  
datalegnth = round(datalegnth);
```

```
%load the saved data files  
eval(['load ',filenameoff]);  
data_off = obj.data;  
t_off = obj.t;  
clear obj.data obj.t
```

```
eval(['load ',filenameon]);  
data_on = obj.data;  
t_on = obj.t;  
clear obj.data obj.t
```

```
% average the data from the tare test  
sig1_off(datalegnth,1) = 0;  
sig2_off(datalegnth,1) = 0;  
sig3_off(datalegnth,1) = 0;
```

```
for j = 1:legnth*freq  
    sig1_off = sig1_off + data_off([(j-1)*datalegnth+1:(j-  
1)*datalegnth+datalegnth],1);  
    sig2_off = sig2_off + data_off([(j-1)*datalegnth+1:(j-  
1)*datalegnth+datalegnth],2);  
    sig3_off = sig3_off + data_off([(j-1)*datalegnth+1:(j-  
1)*datalegnth+datalegnth],3);  
end  
sig1AV_off = [sig1_off/(legnth*freq); sig1_off/(legnth*freq);  
sig1_off/(legnth*freq)];  
sig2AV_off = [sig2_off/(legnth*freq); sig2_off/(legnth*freq);  
sig2_off/(legnth*freq)];  
sig3AV_off = [sig3_off/(legnth*freq); sig3_off/(legnth*freq);  
sig3_off/(legnth*freq)];
```

```
time = t_off([1:datalegnth*3]);
```

```

maxpos_off = max(sig1AV_off);
minpos_off = min(sig1AV_off);
checkpoint_off = (maxpos_off+minpos_off)/2;

k = 1;
r = 1;

% shift the data from the tare test such that x(0) = 0
for m = 1:datalegnth*2-1
    if (sig1AV_off(r) > checkpoint_off) & (sig1AV_off(r+1) <
checkpoint_off) & (k ==1)
        crosspoint1_off = m;
        k = k + 1;
    end
    if (sig1AV_off(r) < checkpoint_off) & (sig1AV_off(r+1) >
checkpoint_off) & (k==2)
        crosspoint2_off = m;
        k = k + 1;
    end
    r = r + 1;
end

start_off = (crosspoint1_off + crosspoint2_off)/2;
start_off = round(start_off);

sig1single_off =
sig1AV_off([start_off+(round(datalegnth/4)):start_off+datalegnth+(ro
und(datalegnth/4))-1]);
sig2single_off =
sig2AV_off([start_off+(round(datalegnth/4)):start_off+datalegnth+(ro
und(datalegnth/4))-1]);
sig3single_off =
sig3AV_off([start_off+(round(datalegnth/4)):start_off+datalegnth+(ro
und(datalegnth/4))-1]);

t = 0:(1/freq)/datalegnth:1/freq;

% average the data from the rotors-on test
sig1_on(datalegnth,1) = 0;
sig2_on(datalegnth,1) = 0;
sig3_on(datalegnth,1) = 0;

for j = 1:legnth*freq
    sig1_on = sig1_on + data_on([(j-1)*datalegnth+1:(j-
1)*datalegnth+datalegnth],1);
    sig2_on = sig2_on + data_on([(j-1)*datalegnth+1:(j-
1)*datalegnth+datalegnth],2);
    sig3_on = sig3_on + data_on([(j-1)*datalegnth+1:(j-
1)*datalegnth+datalegnth],3);
end
sig1AV_on = [sig1_on/(legnth*freq); sig1_on/(legnth*freq);
sig1_on/(legnth*freq)];
sig2AV_on = [sig2_on/(legnth*freq); sig2_on/(legnth*freq);
sig2_on/(legnth*freq)];

```

```

sig3AV_on = [sig3_on/(legnth*freq); sig3_on/(legnth*freq);
sig3_on/(legnth*freq)];

time = t_on([1:datalegnth*3]);

maxpos_on = max(sig1AV_on);
minpos_on = min(sig1AV_on);
checkpoint_on = (maxpos_on+minpos_on)/2;

k = 1;
r = 1;

% shift the rotors on test such that x(0) = 0
for m = 1:datalegnth*2-1
    if (sig1AV_on(r) > checkpoint_on) & (sig1AV_on(r+1) <
checkpoint_on) & (k ==1)
        crosspoint1_on = m;
        k = k + 1;
    end
    if (sig1AV_on(r) < checkpoint_on) & (sig1AV_on(r+1) >
checkpoint_on) & (k==2)
        crosspoint2_on = m;
        k = k + 1;
    end
    r = r + 1;
end

start_on = (crosspoint1_on + crosspoint2_on)/2;
start_on = round(start_on);

sig1single_on =
sig1AV_on([ (start_on+(round(datalegnth/4))):(start_on+datalegnth+(ro
und(datalegnth/4))-1)]);
sig2single_on =
sig2AV_on([ (start_on+(round(datalegnth/4))):(start_on+datalegnth+(ro
und(datalegnth/4))-1)]);
sig3single_on =
sig3AV_on([ (start_on+(round(datalegnth/4))):(start_on+datalegnth+(ro
und(datalegnth/4))-1)]);

t = 0:(1/freq)/datalegnth:(1/freq)-((1/freq)/datalegnth);

%lines below take the one oscillation worth of data and use the
%fast Fourier transform to convert it into frequency based data. we
%then remove the terms corresponding to higher harmonics and invert
%the Fourier transform to obtain the Fourier series approximation of
%the signal with only the desired number of terms included.

F2_off = fft(sig2single_off);
F2_on = fft(sig2single_on);

```

```

F3_off = fft(sig3single_off);
F3_on = fft(sig3single_on);

T2_off = F2_off;
T2_on = F2_on;

T3_off = F3_off;
T3_on = F3_on;

%lines below plot the response in the frequency domain so we can see
%what terms in the fourier series approximation contribute to the
%response

PT2_off = T2_off.*conj(T2_off)/datalegnth;
PT3_off = T3_off.*conj(T3_off)/datalegnth;
f = datalegnth*(0:(datalegnth/2))/datalegnth;

sinpart2_off = imag(T2_off(2))*2/datalegnth;
cospart2_off = real(T2_off(2))*2/datalegnth;
sinpart2_on = imag(T2_on(2))*2/datalegnth;
cospart2_on = real(T2_on(2))*2/datalegnth;

sinpart3_off = imag(T3_off(2))*2/datalegnth;
cospart3_off = real(T3_off(2))*2/datalegnth;
sinpart3_on = imag(T3_on(2))*2/datalegnth;
cospart3_on = real(T3_on(2))*2/datalegnth;

mag2_off = (sinpart2_off^2 + cospart2_off^2)^.5;
phase2_off = atan(cospart2_off/sinpart2_off);
mag2_on = (sinpart2_on^2 + cospart2_on^2)^.5;
phase2_on = atan(cospart2_on/sinpart2_on);

mag3_off = (sinpart3_off^2 + cospart3_off^2)^.5;
phase3_off = atan(cospart3_off/sinpart3_off);
mag3_on = (sinpart3_on^2 + cospart3_on^2)^.5;
phase3_on = atan(cospart3_on/sinpart3_on);

mf_off = [mag2_off;phase2_off;mag3_off;phase3_off];
mf_on = [mag2_on;phase2_on;mag3_on;phase3_on];

%lines below use the FFT to filter the results by setting higher
%frequency terms = 0

T2_on(terms+2:datalegnth-terms) = 0;
T2_off(terms+2:datalegnth-terms) = 0;

T3_on(terms+2:datalegnth-terms) = 0;
T3_off(terms+2:datalegnth-terms) = 0;

```

```
T2_on(1) = 0;
T3_on(1) = 0;

T2_off(1) = 0;
T3_off(1) = 0;

U2_on = ifft(T2_on);
U2_off = ifft(T2_off);

U3_on = ifft(T3_on);
U3_off = ifft(T3_off);

U_off = [U2_off U3_off];
U_on = [U2_on U3_on];

aero2_filt = U2_on - U2_off;
aero3_filt = U3_on - U3_off;
```


Appendix B: MATLAB Program Code, “mavavD”

```
% program calls saved data files for a tare test and a rotors on
%test. Then sends these files to mavplotDZ which returns an
%averaged data set one oscillation length long. This averaged data
%is then used to find the magnitude and phase of the aerodynamic
%component of the data. Correlation between the aerodynamic data
%and the forced velocity perturbation is also calculated. Finally
%the results are converted using the calibration values for the test
%stand.

clear all

base_off = 'dan_tuesnight_13Hz_7in_806ps_tare'; %base name for tare
%tests
base_on = 'dan_tuesnight_13Hz_7in_806ps_124free'; %base name for
%rotors-on tests
sampPERsec = 806; %rate at which the data in the files above was
%taken
freq = 1.3; %frequency of the force oscillation for the tests above
amp = 3.5; %amplitude in inches of forced oscillation
legnth = 180; %legnth in seconds of above tests
numtests = 1; %number of tests taken
freq_retained = 10; %highest frequency content that is retained in
%FFT
terms = round(freq_retained/freq); %number of terms in the final
%FFT representation of the results

TOP_cal = .011284; %calibration factors to convert to N*m
BOT_cal = .041837;

for i = 1:numtests
    n = i;
    file_off = [base_off int2str(n)];
    file_on = [base_on int2str(n)];
    [magphase_off(:,n),magphase_on(:,n),U_off(:, :,n),U_on(:, :,n),t]
= eval('mavplotDZ(file_off,file_on,sampPERsec,freq,legnth,terms)');
end

%lines below average the results from each of the data files to give
%one oscillations worth of data from all files combined

mean_magphase_off = mean(magphase_off,2);
mean_magphase_on = mean(magphase_on,2);

mean_U_off = mean(U_off,3);
mean_U_on = mean(U_on,3);
```

```

mean_aero = mean_U_on - mean_U_off; %gives average aerodynamic
%response

%lines below plot all of the tare tests and all of the rotors-on
%tests on one plot respectively so any outlying tests can be
%observed

figure
hold on
for b = 1:numtests
    plot(t,U_off(:,1,b))
end
figure
hold on
for b = 1:numtests
    plot(t,U_on(:,1,b))
end

datalegnth = sampPERsec*(1/freq); %number of samples in one
%oscillation of data
datalegnth = round(datalegnth);

%lines below take the fft of the aerodynamic data

Faero1 = fft(mean_aero(:,1));
Faero2 = fft(mean_aero(:,2));

Taero1 = Faero1;
Taero2 = Faero2;

f = datalegnth*(0:(datalegnth/2))/datalegnth; %vector of frequency
%components in the fft

%lines below find the sin and cosine components of the first term
%approximation to each signal

sinpart_aero1 = imag(Taero1(2))*2/datalegnth;
cospart_aero1 = real(Taero1(2))*2/datalegnth;

sinpart_aero2 = imag(Taero2(2))*2/datalegnth;
cospart_aero2 = real(Taero2(2))*2/datalegnth;

%lines below find the magnitude of the first term approximation

mag_aero1 = (sinpart_aero1^2 + cospart_aero1^2)^.5;
mag_aero2 = (sinpart_aero2^2 + cospart_aero2^2)^.5;

%lines below find the phase of each first term approximation
%relative to the forced velocity perturbation

phase_aero1 = angle((Taero1(2))*2/datalegnth);
if phase_aero1 > 0
    phase_aero1 = phase_aero1 - pi;
else

```

```

    phase_aero1 = phase_aero1 + pi;
end

phase_aero2 = angle((Taero2(2))*2/datalegnth);
if phase_aero2 > 0
    phase_aero2 = phase_aero2 - pi;
else
    phase_aero2 = phase_aero2 + pi;
end

Amp = 7*.0254/2; %oscillation amplitude in meters
omega = freq*2*pi;
rad_per_samp = omega/sampPERsec;
position_single = Amp*sin(omega*t);
velocity_single = Amp*omega*cos(omega*t);
acc_single = -Amp*omega^2*sin(omega*t);

%lines below shift the aerodynamic responses so that they line up
%with the forced velocity pertubation (phase delay is removed), thus
%the correlation coefficient can be found without being affected by
%the phase delay.

mean_aero1_extend = [mean_aero(:,1); mean_aero(:,1)];
mean_aero(:,1)];
mean_aero2_extend = [mean_aero(:,2); mean_aero(:,2)];
mean_aero(:,2)];

shift1 = round(phase_aero1/rad_per_samp);
shift2 = round(phase_aero2/rad_per_samp);

shifted1 = mean_aero1_extend((datalegnth+1 - shift1):(2*datalegnth -
shift1));
shifted2 = mean_aero2_extend((datalegnth+1 - shift2):(2*datalegnth -
shift2));

%lines below find the correlation coefficient between the forced
%velocity pertubation and the resulting aerodynamic response signal.

corr1 = corrcoef(velocity_single,shifted1);
corr2 = corrcoef(velocity_single,shifted2);

corrvect = [corr1(2); corr2(2)];

%vector of results
mf_aero = [freq; amp; mag_aero1; phase_aero1*180/pi; mag_aero2;
phase_aero2*180/pi; corrvect];

%lines below use the calibration data to convert the above results
%into meaningful units.

TOP_mag = mf_aero(3)*TOP_cal/(amp*omega*.0254);
BOT_mag = mf_aero(5)*BOT_cal/(amp*omega*.0254);

```

```
top_rotor_offset = .109982; %distance from rotor center to top
%strain gauge array in meters
bot_rotor_offset = .173482; %distance from rotor center to bottom
%strain gauge array in meters

moment = (TOP_mag -
((BOT_mag*top_rotor_offset)/bot_rotor_offset))/(1 -
(top_rotor_offset/bot_rotor_offset));
force = (BOT_mag - moment)/bot_rotor_offset;

results = [moment; force];
```

Bibliography

- [1] Schueler, C.J., Ward, L.K. and Hodapp, A.E., "Techniques for Measurement of Dynamic Stability Derivatives in Ground Test Facilities," AGARDograph 121, 1967.
- [2] Bohorquez, F. and Pines, D., "Hover Performance and Swashplate Design of a Coaxial Rotary Wing Micro Air Vehicle," Proceedings of the AHS 60th Forum, Baltimore, MD, June 7-10, 2004.
- [3] Bohorquez, F., Samuel, P., Sirohi, J., Rudd, L., Pines, D. and Perel, R., "Design, Analysis and Performance of a Rotary Wing MAV," Journal of the American Helicopter Society, Vol. 48, No. 2, pp. 80-90, April, 2003.
- [4] Samuel, P., Sirohi, J., Rudd, L., Pines, D. and Perel, R., "Design and Analysis of a Micro Coaxial Rotorcraft," Proceedings of the AHS Vertical Lift Aircraft Design Conference, San Francisco, CA, January 19-21, 2000.
- [5] Hamel, P and Jategaonkar, R., "Evolution of Flight Vehicle System Identification," Journal of Aircraft, Vol. 33. No. 1, 1996, pp. 9-28.
- [6] Amer, B. K. and Gustafson, F. B., "Charts for Estimation of Longitudinal-Stability Derivatives in Forward Flight," NASA TN 2309, 1951.
- [7] Prouty, R. W., Helicopter Performance Stability and Control, PWS Engineering, 1986.
- [8] Smith, G. D., Numerical Solution of Partial Differential Equations, Finite Difference Methods, 3rd Edition, Oxford University Press, 1985.
- [9] Shlager, K. L., and Schneider, J. B., "A Selective Survey of the Finite-Difference Time-Domain Literature," IEE Antennas and Propagation Magazine, Vol. 37, No. 4, August 1995.
- [10] Jategaonkar, R. V., and Thielecke, F., "Aircraft Parameter Estimation – A Tool for Development of Aerodynamic Databases," Sadhana, Vol. 25, Part 2, April 2000.
- [11] Webster, R. S., Chen, J. P., and Whitfield, D. L., "Numerical Simulation of a Helicopter Rotor in Hove and Forward Flight," 33rd Aerospace Sciences Meeting and Exhibit, Reno, NV, January 9-12, 1995.

- [12] Ballhaus, W. F., and Goorjian, P. M., "Implicit Finite-Difference Computations of Unsteady Transonic Flows about Airfoils," *AIAA Journal*, Vol. 15, No. 12, 1978.
- [13] Celi, R., "Optimum Design of Helicopter Rotors for Longitudinal Handling Qualities Improvement in Forward Flight," *AIAA/ASME/ASCE/AHS/ASC 30th Structures, Structural Dynamics and Materials Conference*, Mobile, AL, April 3-5 1989.
- [14] Theodore, C., and Celi, R., "Flight Dynamic Simulation of Hingeless Rotor Helicopters Including a Maneuvering Free Wake Model," *American Helicopter Society 54th Annual Forum*, Washington, D. C., May 20-22, 1998.
- [15] Tischler, M. B., "System Identification Requirements for High_Bandwidth Rotorcraft Flight Control System Design," *Journal of Guidance*, Vol. 13, No. 5, Sept-Oct, 1990.
- [16] Hamel, P and Jategaonkar, R., "Advances In Rotorcraft System Identification," *Progress in Aerospace Sciences*, Vol. 33, pp. 259-284, 1997.
- [17] Chen, R. T. N. and Tischler, M. B., "The Role of Modeling and Flight Testing in Rotorcraft Parameter Identification," *The 1986 AHS Forum, System Identification Session*, Washington, D.C., 1986.
- [18] Tischler, M. B., "System Identification Methods for Flight Control Development and Validation." *Advances in Aircraft Flight Control*. Taylor & Francis, 1996.
- [19] Tischler, M. B., Williams, J. N., and Ham, J. A., "Flight Test Manual, Rotorcraft Frequency Domain Testing," *U.S. Army Aviation Technical Test Center, AQTG Project No. 93-14*, September, 1995.
- [20] Theodore, C. R., Tischler, M. B., and Colbourne, J. D., "Rapid Frequency-Domain Modeling Methods for Unmanned Aerial Vehicle Flight Control Applications," *Journal of Aircraft*, Vol. 41. No. 4, 2004, pp 735-743.
- [21] Shim, D. H., Kim, J. H., and Sastry, S., "Control System Design for Rotorcraft-based Unmanned Aerial Vehicles using Time-domain System Identification," *Proceedings of the 2000 IEEE International Conference on Control Applications*, Anchorage, AK, September 25-27, 2000.
- [22] Mettler, B., *Identification Modeling and Characteristics of Miniature Rotorcraft*, Kluwer Academic Publishers, 2003.

- [23] Mettler, B., Tischler, M. B. and Kanade, T., "System Identification of Small-Size Unmanned Helicopter Dynamics," American Helicopter Society 55th Forum, Montreal, Quebec, Canada, May 1999.
- [24] Kim, S. K. and Tilbury, D. M., "Mathematical Modeling and Experimental Identification of an Unmanned Helicopter Robot with Flybar Dynamics," Journal of Robotic Systems, Vol. 21, No. 3, 2004, pp. 95-116.
- [25] Lee, Y., Kim, S., Suk, J., Koo, H., and Kim, J., "System Identification of Unmanned Aerial Vehicle from Automated Flight Tests," AIAA's 1st Technical Conference and Workshop on Unmanned Aerospace Vehicles, Portsmouth, VA, 2002.
- [26] von der Decken, J., Schmidt, E. and Schulze B., "On the Test Procedures of the Derivative Balances Used in West Germany," AGARD Report No. N79-15061 06-08, AGARD FDP Symposium on Dynamic Stability Parameters, Paper 6, 1978.
- [27] Burt, G. E., "Forced-Oscillation Test Mechanism for Measuring Dynamic-Stability Derivatives in Roll," Journal of Aircraft, Vol. 12, No. 1, January 1975.
- [28] Orlick-Ruckemann, K.J., Adams, P. A., and LaBerge, J. G., "Dynamic Stability Testing of Unconventional Configurations," Journal of Aircraft, Vol. 9, No. 2, February, 1972.
- [29] Alemdaroglu, N., Iyigun, I., Altun, M., Uysal, H., Quagliotti, F., and Guglieri, G., "Determination of Dynamic Stability Derivatives Using Forced Oscillation Technique," Paper Number AIAA 2002-0528, Proceedings of the 40th Aerospace Sciences Meeting and Exhibit, Reno, NV, January 14-17,2002.
- [30] Hanff, E. S., Kapoor, K., Anstey, C. R., and Prini, A., "Large-Amplitude High-Rate Roll Oscillation System for the Measurement of Non-Linear Airloads," AIAA 16th Aerodynamic Ground Testing Conference, Seattle, WA, June 18-20, 1990.
- [31] Kalviste, J., "Use of Rotary Balance and Forced Oscillation Test Data in Six Degrees of Freedom Simulation," AIAA 9th Atmospheric Flight Mechanics Conference, San Diego, CA, August 9-11, 1982.
- [32] Piatak, D. J., and Cleckner, C. S., "A New Forced Oscillation Capability for the Transonic Dynamics Tunnel," 40th AIAA Aerospace Sciences Meeting and Exhibit, Reno, NV, January 14-17, 2002.
- [33] Kay, J., "Acquiring and Modeling Unsteady Aerodynamic Characteristics," AIAA Atmospheric Flight Mechanics Conference, Denver, CO, August 14-17, 2000.

- [34] Murphy, P. C., and Klein, V., "Estimation of Aircraft Unsteady Aerodynamic Parameters from Dynamic Wind Tunnel Testing," American Institute of Aeronautics and Astronautics, Paper AIAA-2001-4016, 2001.
- [35] Uselton, J. C., and Uselton, B. L., "Validity of Small-Amplitude Oscillation Dynamic-Stability Measurement Technique," *Journal of Spacecraft*, Vol, 13, No. 5, 1976.
- [36] Murphy, P. C., and Klein, V., "Validation of Methodology for Estimating Aircraft Unsteady Aerodynamic Parameters from Dynamic Wind Tunnel Tests," AIAA Atmospheric Flight Mechanics Conference and Exhibit, Austin, TX, August 11-14, 2003.
- [37] Orlick-Ruckemann, K.J., "Techniques for Dynamic Stability Testing in Wind Tunnels," AGARD Report No. N79-15061 06-08, AGARD FDP Symposium on Dynamic Stability Parameters, Paper 1, 1978.
- [38] Padfield, G. D., *Helicopter Flight Dynamics: The Theory and Application of Flying Qualities and Simulation Modeling*, AIAA Education Series, 1995.
- [39] Ramirez, R. W., *The FFT Fundamentals and Concepts*, Tektronix, Inc., 1985.
- [40] Bendat, J.S., and Piersol, A.G., *Engineering Applications of Correlation and Spectral Analysis*, 2nd Edition, John Wiley & Sons, Inc., 1993.
- [41] Bendat, J.S., and Piersol, A.G., *Random Data Analysis and Measurement Procedures*, 2nd Edition, John Wiley & Sons, Inc., 1986.
- [42] Roskam, J., *Airplane Flight Dynamics and Automatic Flight Controls*, Design, Analysis and Research Corporation, 1995.
- [43] Leishman, J. G., *Principles of Helicopter Aerodynamics*, Cambridge University Press, 2000.
- [44] Chen, R. T. N., "Effects of Primary Rotor Parameters on Flapping Dynamics," NASA Technical Paper 1431, January 1980.
- [45] Chen, R. T. N., "A Simplified Rotor System Mathematical Model for Piloted Flight Dynamics Simulation," NASA Technical Memorandum 78575, May 1979.